Transportation Research Part C 157 (2023) 104399

Contents lists available at ScienceDirect

Transportation Research Part C

journal homepage: www.elsevier.com/locate/trc

Optimal deployment of an equitable CAV platoonable corridor on road networks with mixed traffic flow

Dan Zhu [a], Tingting Xie [b,d], Yang Liu [b,a,*], Bo Zou [c], Napat Rujeerapaiboon [a]

[a] Department of Industrial Systems Engineering and Management, National University of Singapore, Singapore
[b] Department of Civil and Environmental Engineering, National University of Singapore, Singapore
[c] Department of Civil, Materials, and Environmental Engineering, University of Illinois Chicago, USA
[d] Institute of High Performance Computing (IHPC), Agency for Science, Technology and Research (A*STAR), Singapore

ARTICLE INFO

Keywords:
Connected and autonomous vehicles
Mixed traffic flow
CAV platoonable corridor
Bi-level program
Equity

ABSTRACT

Connected and autonomous vehicle (CAV) technology is expected to increase road capacity and reduce fuel consumption, but it may take time for all human-driven vehicles (HVs) to be replaced by CAVs. During the transition period, CAVs and HVs will continue to coexist. This paper aims to find an optimal deployment of a CAV platoonable corridor to facilitate CAV platooning and better manage traffic congestion on road networks with a mixed traffic flow of CAVs and HVs. Generally, dedicated infrastructure for CAVs, such as CAV lanes, zones, or corridors, may have distributional welfare effects on travelers. Especially, HV users may be worse off because road space is partially converted to dedicated infrastructure for CAVs. To facilitate equitable infrastructure planning, we develop a bi-level program for a Stackelberg game that incorporates the equity concern, where the planner acts as the leader to determine the optimal deployment of an equitable CAV platoonable corridor at the upper level, while travelers are followers who make user-optimal route choices given the CAV platoonable corridor at the lower level. For the lower-level problem, we model the decision-making of travelers as a platoon-embedded network equilibrium with mixed flow (PNEMF) and derive its equivalent variational inequality (VI) problem. The existence and the uniqueness of the VI solution are proved. To solve the bi-level program efficiently, we propose a simulated-annealing-based corridor search (SACS) algorithm. Our numerical experiments on the Nguyen–Dupuis (ND), Sioux Falls (SF), Anaheim, and Winnipeg networks demonstrate the expected benefits of deploying a CAV platoonable corridor if the CAV market penetration ratio exceeds a certain threshold. In the meantime, both CAV and HV users are better off with the deployed equitable corridor. In addition, we find that the degree of the transportation planner's concern about the inequity issue has a significant impact on the corridor design when the CAV penetration ratio is low. With less concern about the inequity issue, the CAV platoonable corridor is longer and more HVs experience higher generalized travel costs.

1. Introduction

Connected and autonomous vehicles (CAVs) are expected to bring significant benefits to human mobility. Compared to conventional human-driven vehicles (HVs), CAVs can communicate in real-time with other vehicles (vehicle-to-vehicle (V2V)), infrastructure (vehicle-to-infrastructure (V2I)), and network through wireless communication technologies (Molina-Masegosa and

* Corresponding author at: Department of Civil and Environmental Engineering, National University of Singapore, Singapore.
E-mail address: ceelya@nus.edu.sg (Y. Liu).

https://doi.org/10.1016/j.trc.2023.104399
Received 21 December 2022; Received in revised form 23 October 2023; Accepted 23 October 2023
Available online 6 November 2023
0968-090X/

Gozalvez, 2017). In addition, the introduction of automated driving systems reduces human-related driving errors and smooths the traffic flow. As a result, CAVs will not only travel more efficiently and safely (Farah and Koutsopoulos, 2014; Khattak and Wali, 2017), but also can move in a group with reduced headway, which is referred to as *CAV platooning* (Shladover et al., 2015). Platooning has two main operational advantages over traveling individually. First, road capacity will increase due to reduced headway between CAVs within a platoon compared to the headway between HVs of today (*e.g.*, Shladover et al. (2012), Zhao and Sun (2013)). Second, traveling closer reduces air drag for CAVs in a platoon, and consequently, vehicle energy consumption and travel cost (McAuliffe et al., 2018; Bibeka et al., 2021).

Considering these benefits of platooning, existing research has looked into platoon trajectory optimization on arterial roads, in a 100% CAV environment using simulated-based experiments (Liu et al., 2019; Feng et al., 2019). However, the survey by Litman (2020) pointed out that it would take several decades to achieve a high penetration ratio of fully automated vehicles. In other words, HVs and CAVs will coexist on roads for a long time. During this period of coexistence, the interaction between CAVs and HVs in mixed traffic may hamper the formation and movement of CAV platoons. Human drivers tend to overreact when driving close to the preceding vehicle, exhibiting elevated emotions, deviations from normal traffic speeds, and deliberate violations (Lee et al., 2021). Such aggressive actions can trigger traffic oscillations (Laval and Leclercq, 2010; Gong et al., 2016). To circumvent the challenges brought by mixed CAV/HV movement while reaping the benefits of CAV platooning, a potential solution is to deploy CAV-dedicated facilities to separate CAV from HV traffic, at least in part of the road network. Motivated by this idea, this paper proposes the concept of *CAV platoonable corridor*, which is equipped with advanced wireless communication and data transfer systems. Although some existing literature pointed out that CAVs could platoon via V2V communication in a pure CAV environment (Darbha et al., 2018; Zeng et al., 2019), a potential issue for this cooperative adaptative control system is the communication failure due to communication interference or information congestion (Kim et al., 2017; Wang et al., 2018), particularly under heavy traffic (He et al., 2017). By contrast, V2I can provide high-reliability and low-latency communication with the assistance of edge and central cloud computing (Chang and Chiou, 2019; Hu et al., 2019). Therefore, the planner should upgrade infrastructure to achieve V2I communication on the corridor, which can ensure efficient and effective message dissemination for platooned CAVs (Molina-Masegosa and Gozalvez, 2017), especially in a dense platoon-embedded traffic environment (Lin and Rubin, 2017). Thanks to V2I communication technology, the deployed corridor enables CAVs to travel uninterrupted as platoons for long distances on consecutive links, even in dense traffic scenarios. To fully exploit the benefits of the deployed corridor in facilitating CAV platooning, we consider the CAV platoonable corridor to be deployed on highways and urban expressways, which are designed to handle large, high-speed traffic over long and uninterrupted distances.

The deployment of a CAV platoonable corridor may bring distributional welfare effects across different road users. Therefore, transportation planners need to consider the inequity issue when planning the corridor. On the one hand, CAVs will take full advantage of the embedded wireless equipment to efficiently and safely platoon while traveling on the corridor. On the other hand, as HVs are not allowed to use links on the corridor, they could be adversely affected by experiencing higher travel costs due to fewer path options. To find an optimal CAV platoonable corridor with the inequity issue incorporated, we develop a bi-level program to model the problem as a Stackelberg "leader–follower" game. At the upper level, the transportation planner *leads* the road users through deploying an equitable CAV platoonable corridor. The deployment of a CAV platoonable corridor can be influenced by the CAV market penetration ratio, network topology, platoon size, link characteristics, demand level, and more importantly, route choices for both CAVs and HVs. Therefore, at the lower level, we capture it by letting road users *follow* by making their user-optimal route choices given the CAV platoonable corridor. This bi-level structure allows the leader to account for the followers' routing choices. By conducting this study, we aim to answer the following questions:

- How will the CAV platoonable corridor affect travelers' route choices and the spatial distribution of traffic congestion in the long run?
- How to optimally determine a CAV platoonable corridor considering both system efficiency and equity?
- How will the CAV penetration ratio, the degree of planner's concern about the equity, the platoon size, and the demand level affect the deployment of the CAV platoonable corridor?

1.1. Literature review

The related literature can be divided into two streams. The first stream focuses on infrastructure planning for promoting the adoption of autonomous vehicles (AVs) in a mixed–traffic environment. Chen et al. (2016) discussed how, when, and where to deploy AV-dedicated lanes to adapt to various AV market penetration ratios. Liu and Song (2019) adopted a mixed strategy of AV-dedicated lanes and autonomous vehicle/toll lanes to nurture the AV market. They showed that this combined strategy could significantly improve system performance even if the AV penetration ratio is low. Last but not least, Ye and Wang (2018) compared the performances of deploying AV lanes and implementing congestion pricing. They found that the former was superior to the latter when the AV penetration ratio was sufficiently high.

Other studies consider introducing an exclusive AV zone/subnetwork to boost the AV market penetration ratio. Chen et al. (2017b) first developed a mixed network equilibrium model by assuming that AVs and HVs outside of the AV zone (*i.e.,* a cordon-based subnetwork) follow user equilibrium (UE) principle to minimize each individual's travel time while AVs within the AV zone follow system optimum (SO) with a collective goal of minimizing the total travel time. A bi-level programming model was then proposed to optimize the AV zone design with the mixed network equilibrium being the lower-level problem. Their numerical results indicated that deploying an AV zone could substantially reduce the system travel time. Recently, Madadi et al. (2020) selected

a connected subnetwork based on safety and quality considerations, in which fully autonomous driving of AVs with levels 3–4 can be realized, while manual driving is compulsory for the remaining roads. All the above-mentioned studies do not specifically point out whether AVs are equipped with connected technologies to achieve V2V/V2I technologies since they do not focus on how infrastructure planning influences vehicle platooning. To the best of our knowledge, we are the first to investigate the planning of transportation infrastructure for facilitating vehicle platooning. To consider the impacts of the CAV platoonable corridor on travelers' route choices and the resultant distribution of traffic congestion, we introduce the traffic equilibrium with CAVs and HVs that explicitly take platooning characteristics into consideration. Considering that CAVs/HVs are generally owned by different companies or individuals, we assume that they make route choices following the UE principle.

The second stream is about vehicles' coordination and formation of a platoon. Liang et al. (2015) studied how to adjust speed to form platoons in a fuel-efficient manner. Zhang et al. (2017) investigated the influence of uncertain travel time on vehicle platooning. Larsen et al. (2019) allowed vehicle platooning to be formed at the hub alongside the motorway network and proposed a computationally effective heuristic algorithm to explore the profitability of hub-based vehicle platooning. Abdolmaleki et al. (2019) examined the scheduled platoon planning by simultaneously optimizing departure time, routing, and spacing. Different from the studies mentioned above, which assume that vehicles act collectively, Johansson et al. (2018) explored how each vehicle can behave individually and decide its individual departure time. They considered that each vehicle makes a trade-off between the benefit of the reduced travel time due to platooning and the disbenefit of platoon formation delay. All the studies above investigate vehicle platooning from a microscopic perspective. From a macroscopic perspective, Noruzoliaee et al. (2021) studied spontaneous truck platooning. They developed a network equilibrium model to analyze how truck platooning influences the fuel consumption of trucks and road capacity when non-platooning vehicles coexist on roads. We study vehicle platooning on road networks with the mixed traffic flow of HVs and CAVs using an equilibrium model. However, our work differs from Noruzoliaee et al. (2021) in two significant ways. First, they consider truck platooning on links where other types of vehicles coexist over the whole network, while we consider the platooning of CAVs on a designated corridor to avoid interference from uncontrolled HVs. Second, Noruzoliaee et al. (2021) only consider a mixed equilibrium problem, while we investigate not only users' route choices and the resultant traffic congestion distribution on road networks with CAV platooning, but also the optimal deployment of an equitable CAV platoonable corridor.

1.2. Contributions and organization

The contributions of the paper can be summarized as follows.

- We make the first attempt to study the optimal deployment of an equitable CAV platoonable corridor on a road network with mixed traffic of CAVs and HVs. Most existing studies on infrastructure planning for AVs consider deploying dedicated lanes or zone to promote AV market penetration ratio. To our best knowledge, no studies consider the infrastructure planning for CAV platooning under mixed traffic. To fill this research gap, we propose to deploy a CAV platoonable corridor to aggregate CAV flow and better facilitate CAV platooning. Considering a CAV-dedicated infrastructure may adversely affect HVs, the equity concern is incorporated in the decision-making of the corridor deployment to well balance the impacts of the corridor on different travelers. Compared to a CAV-dedicated zone/subnetwork, which may require HVs to make long detours due to the inaccessibility of the whole area for HVs, a CAV platoonable corridor is expected to be more equitable since HVs can still access nodes on the corridor. Moreover, compared to deploying CAV-dedicated links or lanes, which requires CAVs to frequently form and dissolve platoons when traversing different links, a corridor-based design enhances transportation system efficiency by enabling smoother CAV platooning over longer distances without frequent platoon forming and dissolving maneuvers. This approach is particularly attractive on highways or expressways, which usually handle large, high-speed traffic over long, uninterrupted distances. To capture travelers' responses to the long-term planning decisions of corridor deployment, we model the problem as a Stackelberg game and formulate it as a bi-level program, where the lower-level model captures travelers' route choices based on a given corridor (*i.e.*, decisions of the upper-level problem) in the long run.
- For a given CAV platoonable corridor, we propose a platoon-embedded network equilibrium with mixed flow (PNEMF) to characterize route choices of HVs and CAVs and the resulting distribution of traffic congestion on a general road network. In the proposed PNEMF, we consider that CAVs with the same entrance and exit (E–E) pair form and travel in platoons on the CAV platoonable corridor. Although alternative platooning strategies, such as entrance-based platooning or link-based platooning, could be considered, additional inconvenience cost and potential safety concerns could also arise. On the contrary, the proposed E–E-pair-based platooning may be a safer option because of the reduced need for platoon dissolution and reformation. In addition, the plausibly longer waiting time due to CAVs in a platoon having the same entry and exit on the corridor may not be a significant concern under dense traffic, as the platooning benefits, including reduced inconvenience cost, fuel cost, and travel time cost, may outweigh the increased waiting time cost. To avoid interference among different platoon formations on the same road, platoon formation areas alongside possible entrances are introduced for CAVs to form platoons. In addition, we derive the equivalent variational inequality (VI) problem of the PNEMF and prove the existence and uniqueness of the VI solution.
- To efficiently solve the bi-level corridor planning problem, we propose a simulated-annealing-based corridor search (SACS) algorithm, which enables the gauging of the connectivity of CAV platoonable links for being a corridor while searching for the optimal solution. At each iteration, to find a high-quality neighboring solution of the current solution, link addition and deletion heuristic rules are designed and embedded in the proposed SACS to assign weight to each candidate link based on CAV-specific link flows. We test the proposed SACS algorithm on the Nguyen–Dupuis (ND) network and show that the proposed SACS algorithm can efficiently find an optimal CAV platoonable corridor. When solving larger networks, such as the Sioux Falls (SF) network, the Anaheim network, and the Winnipeg network, the computation efficiency remains.

- Our numerical results indicate that the deployed CAV platoonable corridor can benefit both CAVs and (the majority of) HVs when the CAV market penetration ratio exceeds a threshold. Additionally, the degree of the transportation planner's concern about the inequity issue significantly impacts the corridor design when the CAV penetration ratio is low (*e.g.,* 30%). With less concern about the inequity issue, the CAV platoonable corridor becomes longer, and more HVs suffer higher generalized travel costs. Furthermore, the degree of traffic congestion can also influence the design of the CAV platoonable corridor, with more severe congestion leading to a longer corridor. We also compared the performance of a CAV platoonable corridor and a CAV platoonable zone and found that the latter leads to higher generalized travel costs for some HVs, while the former benefits all HVs. This numerical result confirms our expectation that a CAV platoonable corridor is more equitable.

The remainder of the paper is organized as follows. Section 2 presents the model for the lower-level problem, derives its equivalent VI problem, examines its solution properties, and finally presents the model for the investigated Stackelberg game. Section 3 presents a SACS algorithm for efficiently finding an optimal CAV platoonable corridor. A modified path-based gradient projection algorithm is proposed and embedded in the SACS algorithm to solve the lower-level problem for a given corridor. In Section 4, numerical experiments are conducted on the ND, SF, Anaheim, and Winnipeg networks to test the proposed model and solution algorithm. We also make a comparison between a CAV platoonable corridor and a CAV platoonable zone on the ND network to showcase the former's superiority in balancing the positive and negative effects of a CAV-dedicated infrastructure on CAV and HV users. Finally, Section 5 summarizes the main findings, insights, and future extensions.

2. Model formulation

This study aims to deploy an equitable CAV platoonable corridor on a general road network with mixed traffic of CAVs and HVs. In Section 2.1, we describe our research problem. Section 2.2 introduces the model setting and models the lower-level problem for a given CAV platoonable corridor as a PNEMF. In Section 2.3, we formulate the PNEMF as an equivalent VI problem and prove the existence and uniqueness of the VI solution. Section 2.4 defines the objective function of the upper-level problem and presents the bi-level program for determining the optimal deployment of an equitable CAV platoonable corridor, while the impact of the corridor deployment on users' responses (*i.e.,* route choices) are fully considered.

2.1. Problem description

In this study, we define a corridor as a sequence of consecutive links without sub-cycles (*e.g.*, see Fig. 3). The transportation planner selects a subset of links on the road network to upgrade them to CAV platoonable links so as to form a CAV platoonable corridor. The upgrading here refers to equipping the selected road links with advanced communication systems to ensure efficient and smooth CAV platooning on a CAV platoonable corridor. Upgrading infrastructure to enable V2I communication can provide high-reliability and low-latency communication, which is more desirable for CAV platooning in a dense traffic scenario. Furthermore, we expect that providing a CAV platoonable corridor can encourage CAVs to use the corridor, so the advantages of CAV platooning (*e.g.*, improved road capacity and reduced fuel consumption) can be exploited maximally. However, deploying dedicated infrastructure for CAVs, such as CAV lanes, zones, or corridors, may have distributional welfare effects on travelers. Specifically, HV users may experience higher generalized travel costs due to fewer path options and less road space. Considering both the advantages and disadvantages of deploying a CAV platoonable corridor, the objective function of the transportation planner includes the costs of upgrading links to form a CAV platoonable corridor, traffic congestion, and inequity. The inequity cost is measured by the increase (if any) in HVs' total generalized travel costs due to the conversion of the selected links to a CAV platoonable corridor.

To find the optimal deployment of an equitable CAV platoonable corridor, we develop a bi-level program to model the problem as a Stackelberg game as illustrated in Fig. 1. At the upper level, the transportation planner acts as the leader to determine links to be upgraded to CAV platoonable links and form a corridor for minimizing the social cost, which is a weighted average of the sum of first two components (the upgrade cost and travelers' total generalized travel cost at the target year) and the inequity cost at the target year. The transportation planner can adjust the weightage π according to the degree of his/her concern about inequity. Given the deployment of the equitable CAV platoonable corridor, at the lower level, CAVs and HVs act as followers to make route choices aiming to minimize their respective generalized travel costs. The lower-level problem is modeled as a PNEMF. The bi-level structure enables the leader to account for the impact of his/her decision on followers' reactions, *i.e.*, route choices, when the leader determines the optimal deployment of the equitable CAV platoonable corridor.

2.2. Platoon-embedded network equilibrium with mixed flow

2.2.1. Model setting

We first describe the model setting. Let $G = (N^0, A^0)$ denote a network graph with a subgraph $\tilde{G} = (\tilde{N}, \tilde{A})$ representing the CAV platoonable corridor, which is only accessible for CAVs. Note that $N^0 = N \cup \tilde{N}$ and $A^0 = A \cup \tilde{A}$, where N and $\tilde{N}$ denote the set of nodes outside and inside the corridor, and A and $\tilde{A}$ denote the set of non-platoonable links and CAV platoonable links, respectively. Note that A and $\tilde{A}$ are mutually exclusive (*i.e.,* $A \cap \tilde{A} = \emptyset$), N and $\tilde{N}$ may have intersections (*i.e.,* $N \cap \tilde{N} \neq \emptyset$) because a node can serve as both a platoonable and a non-platoonable node. Given a network topology, a CAV platoonable corridor can be represented as a sequence of nodes $(i_1, i_2, \ldots, i_{|\tilde{N}|-1}, i_{|\tilde{N}|})$ such that $(i_1, i_2), (i_2, i_3), \ldots, (i_{|\tilde{N}|-1}, i_{|\tilde{N}|})$ are consecutive CAV platoonable links and i_j is distinct. On a road network with an equitable CAV platoonable corridor, CAVs decide whether to use this corridor and where to

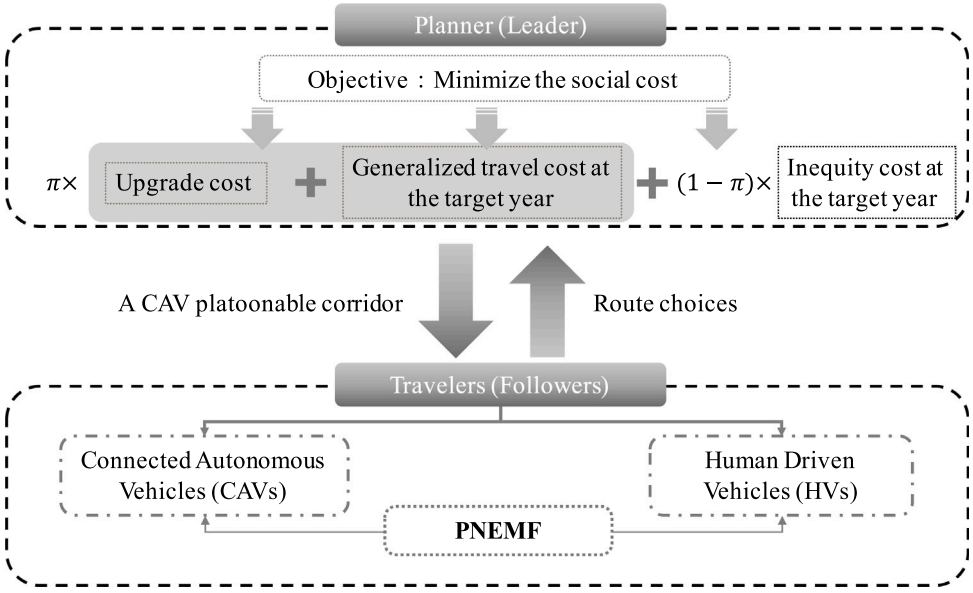

Fig. 1. An illustration of the proposed bi-level program.

enter and exit the corridor, whereas HVs can only use routes consisting of non-platoonable links. Each vehicle is associated with an origin–destination (O–D) pair from $(\tilde{N} \cup N)^2$, and the set of O–D pairs is denoted by W.

Next, we describe the platoon formation process for CAVs that choose to enter the corridor $\tilde{G}$. Let $\tilde{W} \subseteq \tilde{N}^2$ denote the set of admissible entrance–exit (E–E) pairs. A node on the corridor from $\tilde{N}$ is an entrance if a node from $N \backslash \tilde{N}$ is connected to it or if it is an origin. Likewise, a node on the corridor from $\tilde{N}$ is an exit if it is connected to a node from $N \backslash \tilde{N}$ or if it is a destination. Then, for each $\tilde{w} \in \tilde{W}$, we can find a unique path from its entrance $o_{\tilde{w}}$ to its exit $d_{\tilde{w}}$. For ease of exposition, we henceforth denote by $\tilde{w}(:)$ an ordered set of links on E–E pair $\tilde{w}$. Note that we do not have a similar notation $w(:)$ for $w \in W$, as there could be multiple paths between an O–D pair $w \in W$. Given the deployed CAV platoonable corridor, we consider platoons to be formed among CAVs with the same E–E pair for two reasons. First, once formed, a platoon will be maintained while traveling on the corridor, thus avoiding the inconvenience of potentially dissolving and reforming platoons which could occur with link-based platooning. If we do not require platooning CAVs to have the same exits, then some CAVs in a platoon may leave the platoon earlier, which may trigger position adjustment for the remaining CAVs in the platoon (rear CAV(s) to speed up and front CAV(s) to slow down, to fill the gap left by the departing CAV(s)) in order to continue platooning. Such speed adjustment may trigger shockwaves or unsafe traffic situations (Martínez-Díaz et al., 2021). Second, while E–E-pair-based platooning may not be as flexible as link-based or entrance-based platooning and may require longer platoon formation time, the benefit of E–E-pair-based platooning, including reduced inconvenience cost, fuel cost, and travel time cost, can outweigh the increased waiting time cost under dense traffic.

While the development of platoon formation areas may entail the land-use cost, platoon formation areas are perceived essential in this study. This is because having platoon formation in dedicated areas can eliminate the impact of platoon formation processes on CAVs already in platooning, creating a safer and smoother environment for platoon formation and operations than without platoon formation areas. Fig. 2 gives an example of platoon formation in platoon formation areas when the platoon size s is three. It is worth noting that the land-use cost associated with platoon formation areas may not be as high as initially perceived. This is because existing public parking garages, petrol service points, and some parking spaces in cities can be retrofitted with the necessary sensing, computing, and communication devices to become qualified platoon formation areas (Johansson et al., 2021a; Wang et al., 2022; Hall and Chin, 2005).

Fig. 3 gives an example of a CAV platoonable corridor on the ND network. In this example, the sets of nodes inside the corridor and CAV platoonable links are $\tilde{N} = \{4, 5, 6, 7, 8\}$ and $\tilde{A} = \{(4, 5), (5, 6), (6, 7), (7, 8)\}$, respectively. The set of nodes outside the corridor is $N = \{1, 2, 3, 4, 5, 6, 7, 8, 9, 10, 11, 12, 13\}$. The set of non-platoonable links is $A = \{(1, 5), (1, 12), (2, 3), (4, 9), (5, 9), (6, 10), (7, 11), (8, 2), (9, 10), (9, 13), (10, 11), (11, 2), (11, 3), (12, 6), (12, 8), (13, 3)\}$. The set of O–D pair $W = \{(1, 3), (4, 3)\}$, and the E–E pairs are given by

$$\tilde{W} = \{(4, 5), (4, 6), (4, 7), (4, 8), (5, 6), (5, 7), (5, 8), (6, 7), (6, 8)\}.$$

Regarding CAVs platoon formation behavior, CAVs entering the corridor via node 5, for instance, can exit from node 6, node 7, or node 8, but only CAVs with the same E–E pair, such as $(5, 7)$, can platoon together.

To facilitate subsequent discussions, we next introduce several other notations. Let $M = \{CAV, HV\}$ denote the set of vehicle classes. The travel demand of class $m \in M$ between O–D pair $w \in W$ is denoted by $q^{w,m}$. $R^{w,m}$ denotes the set of all feasible paths between O–D pair $w \in W$ for class $m \in M$. We assume that $R^{w,m} \neq \emptyset$ and $q^{w,m} > 0$. Since the corridor is dedicated to CAVs and off limits to HVs, $R^{w,HV}$ and $R^{w,CAV}$ may not be identical. $h_r^{w,m}$ represents the flow of vehicle class m between O–D pair w on path

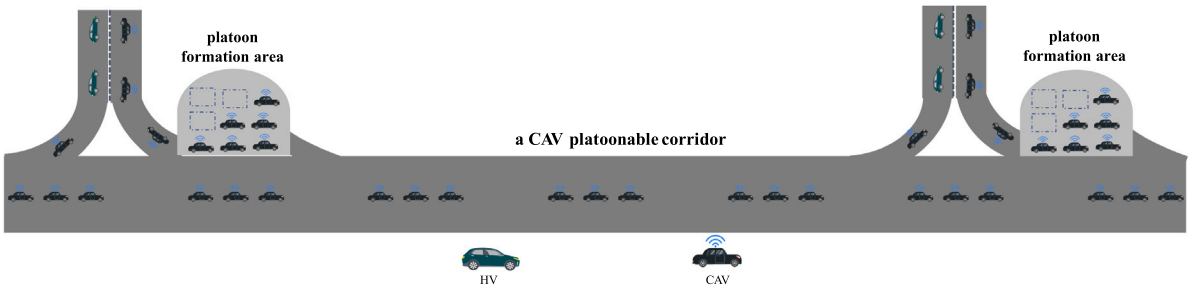

Fig. 2. An example of platoon formation with a platoon size $s = 3$.

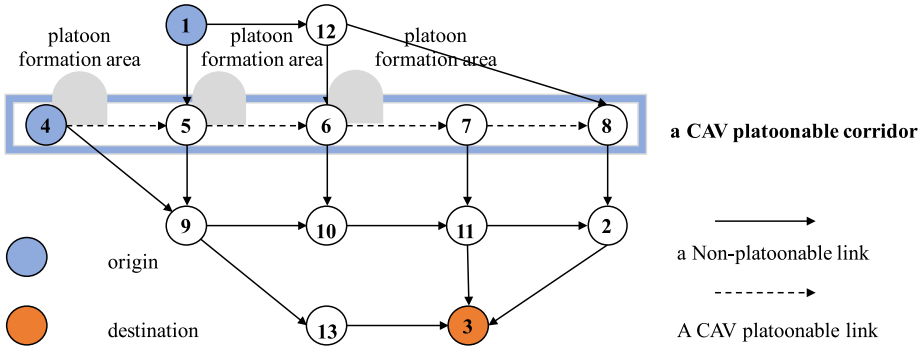

Fig. 3. An example of the CAV platoonable corridor on the ND network.

$r \in R^{w,m}$. Let $a \in A$ represent a non-platoonable link and $a \in \tilde{A}$ represent a CAV platoonable link. We denote $x_a^{w,m}$ as the flow of class $m \in M$ between O–D pair $w \in W$ on a non-platoonable link $a \in A$ and $x_{\tilde{w}}^{w,CAV}$ the flow on E–E pair $\tilde{w} \in \tilde{W}$ by vehicle class CAV. Besides, let v_a^m and $v_{\tilde{w}}^{CAV}$ represent the aggregate flow of class $m \in M$ on a link $a \in A$ and the aggregate flow of CAVs on E–E pair $\tilde{w} \in \tilde{W}$, respectively. Also, we denote v_a as the aggregate flow on a link $a \in A^0$. Then, the vector of path flows $h_r^{w,m}$, the vector of link and E–E pair flows $x_a^{w,m}$, $x_{\tilde{w}}^{w,CAV}$ and the vector of aggregate flow $\mathbf{v}$ that contains all v_a^m, $v_{\tilde{w}}^{CAV}$, v_a can be defined as follows

$$\mathbf{h} = \left(h_r^{w,m}\right)_{r \in R^{w,m}, w \in W, m \in M};$$

$$\mathbf{x} = \left(\left(x_a^{w,m}\right)_{a \in A, w \in W, m \in M}, \left(x_{\tilde{w}}^{w,CAV}\right)_{\tilde{w} \in \tilde{W}, w \in W}\right);$$

$$\mathbf{v} = \left(\left(v_a^m\right)_{a \in A, m \in M}, \left(v_{\tilde{w}}^{CAV}\right)_{\tilde{w} \in \tilde{W}}, \left(v_a\right)_{a \in A^0}\right).$$

For ease of our exposition, the notations are summarized in Table 1.

2.2.2. The generalized travel costs

This subsection defines the generalized travel costs on a non-platoonable link $a \in A$ and an E–E pair $\tilde{w} \in \tilde{W}$. The generalized travel cost consists of the cost of travel time, fuel cost, and platoon-related cost. The platoon-related cost, which only applies to the platooned CAVs, considers the costs of platoon formation time and dissolution time and inconvenience. The formulation of each cost component will be discussed in turn.

The generalized travel cost of using a non-platoonable link $a \in A$ for vehicle class $m \in M$, denoted as g_a^m, is defined as the sum of travel time cost and the fuel cost:

$$g_a^m(v_a) = \underbrace{t_a(v_a)\lambda_m}_{\text{travel time cost}} + \underbrace{f_a^m}_{\text{fuel cost}}, \tag{1}$$

where λ_m is the VoT for users of class $m \in M$.

The generalized travel cost of using an E–E pair $\tilde{w} \in \tilde{W}$ is denoted by $g_{\tilde{w}}^{CAV}$, which includes the travel time cost and fuel cost of CAV platoonable links on this E–E pair $\tilde{w}$ and the platoon-related cost containing the platoon formation time cost, deformation

Table 1
Notations.

Notations	Descriptions
Sets	
N	Set of nodes outside the corridor
A	Set of non-platoonable links
$\tilde{N}$	Set of nodes inside the corridor
$\tilde{A}$	Set of CAV platoonable links
N^0	Set of all nodes (*i.e.*, $N^0 = N \cup \tilde{N}$)
A^0	Set of all links (*i.e.*, $A^0 = A \cup \tilde{A}$)
W	Set of origin–destination (O–D) pairs
$\tilde{W}$	Set of entrance–exit (E–E) pairs for the CAV platoonable corridor
M	Set of classes (*i.e.*, $M = \{CAV, HV\}$)
$R^{w,m}$	Set of feasible paths between O–D pair $w \in W$ by class $m \in M$
Parameters	
$q^{w,m}$	Travel demand between O–D pair $w \in W$ by class $m \in M$ (vehicles/h)
s	Platoon size (number of CAVs per platoon)
λ_m	Value of time (VoT) of vehicle class m ($/h)
l_a	Length of link $a \in A^0$ (miles)
θ_m	Unit fuel price per mile on class m ($/mile)
f_a^m	Fuel cost on link $a \in A^0$ by class m ($)
$\tau_{\tilde{w}}$	Platoon-related cost for E–E pair $\tilde{w} \in \tilde{W}$ ($)
δ	Reduction fuel ratio caused by platoon formation on link $a \in \tilde{A}$
C_a	Capacity of link $a \in A^0$ (vehicles/h)
C_a^0	Capacity of CAV platoonable link $a \in \tilde{A}$ before upgrading (vehicles/h)
t_a^0	Free-flow travel time on link $a \in A^0$ (h)
γ	The proportion between the intra-platoon critical distance and the inter-platoon critical distance
π	The weightage introduced to balance the sum of upgrade cost and total generalized travel cost and the inequity cost
η	The conversion parameter from hour to year
κ	The magnitude of the platoon-related cost compared to free-flow travel time cost
ϵ	The inconvenience cost for one-time platoon ($)
k_a	Investment cost for each CAV platoon link $a \in \tilde{A}$ per mile ($/mile)
Decision variables	
$h_r^{w,m}$	Flow on path $r \in R^{w,m}$ for O–D pair $w \in W$ by class $m \in M$ (vehicles/h)
v_a^m	Aggregate flow on link $a \in A$ by class $m \in M$ (vehicles/h)
$v_{\tilde{w}}^{CAV}$	Aggregate flow on E–E pair $\tilde{w} \in \tilde{W}$ by class CAV (vehicles/h)
v_a	Aggregate flow on link $a \in A^0$ (vehicles/h)
$x_a^{w,m}$	Flow on link $a \in A$ between O–D pair $w \in W$ by class $m \in M$ (vehicles/h)
$x_{\tilde{w}}^{w,CAV}$	Flow on E–E pair $\tilde{w} \in \tilde{W}$ for O–D pair $w \in W$ by class CAV (vehicles/h)
$t_a(v_a)$	Travel time of link $a \in A^0$ (h)
$g_a^m(v_a)$	Generalized travel cost on a non-platoonable link $a \in A$ by vehicle class $m \in M$ ($)
$g_{\tilde{w}}^{CAV}(\mathbf{v})$	Generalized travel cost on an E–E pair $\tilde{w} \in \tilde{W}$ by vehicle class CAV ($)

time cost and inconvenience cost. That is,

$$g_{\tilde{w}}^{CAV}(\mathbf{v}) = \underbrace{\sum_{a \in \tilde{w}(:)} t_a(v_a)\lambda_{CAV}}_{\text{travel time cost}} + \underbrace{\sum_{a \in \tilde{w}(:)} f_a^{CAV}}_{\text{fuel cost}} + \underbrace{\tau_{\tilde{w}}}_{\text{platoon-related cost}}, \tag{2}$$

The first terms of g_a^m and $g_{\tilde{w}}^{CAV}$ are the costs of travel time, which is a product of travel time and VoT for users of class $m \in M$. We assume that the link travel time t_a is a strictly increasing function of the aggregate link flow v_a, and adopt the Bureau of Public Roads (BPR) function (Bureau of Public Roads, 1964) to estimate the travel time t_a on link $a \in A^0$ as follows:

$$t_a(v_a) = t_a^0 \left[1 + \alpha \left(\frac{v_a}{C_a}\right)^{\beta}\right], \tag{3}$$

where t_a^0 and C_a represent the free-flow travel time and the capacity on link $a \in A^0$, respectively, and α and β are default parameters. To be sure, vehicle travel time on a link may not follow exactly the BPR function under mixed traffic.[1] However, there are no well-recognized alternative functions with strong evidence that they would predict link travel time better. Thus, we still consider the

[1] Indeed, there are alternative, albeit more complex, functions intended to better account for traffic overflow situations resulting from high β values. Examples of these functions include the conical volume-delay function proposed by Spiess (1990) and modifications of BPR function, such as BPR2 and BPR3. The functional forms of BPR2 and BPR3 are identical to the BPR function when traffic is low. However, different function shapes will be introduced when traffic is congested (Saric et al., 2019). In the transportation network modeling literature, however, these alternative functional forms are much less widely accepted than the BPR function. If these alternative functions were adopted, the objective function value at the upper level would likely change, as would the platoonable corridor.

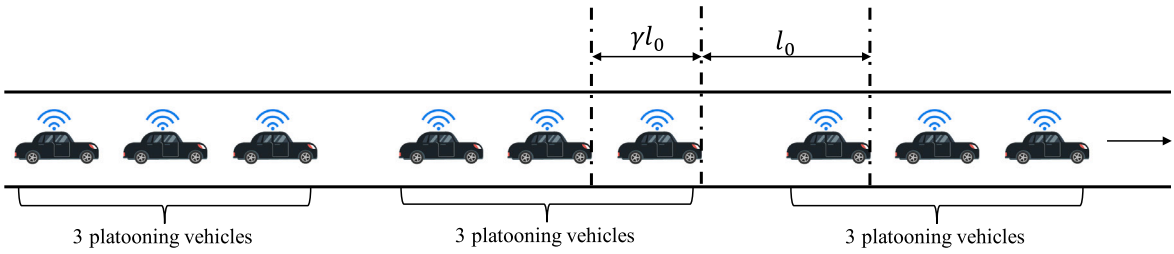

Fig. 4. An illustration of the intra-platoon and inter-platoon critical distances.

BPR function given its simplicity, minimal requirement of input parameters, and wide use in transportation modeling (Mtoi and Moses, 2014).

Next, we elaborate how capacity is characterized in our study. On non-platoonable links outside the corridor, we assume that all vehicles maintain a consistent spacing from their followers regardless of vehicle type, as if they were an HV followed by another HV.[2] For each CAV platoonable link $a \in \tilde{A}$, it is widely considered that CAV platooning can significantly improve road capacity. To quantify the improvement, we employ an analytical approach developed by Chen et al. (2017a) which gives the relationship between C_a^0 (the capacity before upgrading) and C_a (the capacity after upgrading) of a link. To be specific, we denote l_0 as the inter-platoon critical distance and γl_0 $(0 < \gamma < 1)$ as the intra-platoon critical distance that meets the safety requirements imposed by the transportation planner. Fig. 4 illustrates the definitions of l_0 and γl_0 for the case of $s = 3$. It can be seen that, for each $a \in \tilde{A}$, the distance required for s vehicles to travel safely and consecutively reduces from sl_0 to $l_0 + (s-1)\gamma l_0$. Therefore, we have

$$\frac{C_a^0}{C_a} = \frac{1 + (s-1)\gamma}{s}. \tag{4}$$

C_a^0/C_a increases with γ and decreases with s. It should be noted that the capacity of a non-platoonable link $a \in A$, C_a, and the capacity of a CAV platoonable link $a \in \tilde{A}$ before upgrading, C_a^0, will be given in advance. The capacity of a CAV platoonable link $a \in \tilde{A}$ after upgrading, C_a, can be obtained from the above equation once we fix s and γ.

The second terms of g_a^m and $g_{\tilde{w}}^{CAV}$ are the fuel costs. We assume that the fuel cost of traveling through a link is proportional to the link distance. For a non-platoonable link $a \in A$, the fuel cost f_a^m of link a for vehicle class $m \in M$ is estimated as

$$f_a^m = \theta_m l_a, \tag{5}$$

for some vehicle class-specific conversion parameter θ_m $(\theta_m > 0)$. Since platooned CAVs can travel together with less time headway, they are more energy efficient because of the reduced aerodynamic drag. In light of this, we estimate the fuel cost f_a^{CAV} for a CAV traveling on a platoonable link $a \in \tilde{A}$ as

$$f_a^{CAV} = \theta_{CAV} l_a (1 - \delta), \tag{6}$$

for some constant $\delta \in (0, 1)$.

The third term of $g_{\tilde{w}}^{CAV}$ is the platoon-related cost, including the costs of platoon formation, dissolution time, and inconvenience on E–E pair $\tilde{w} \in \tilde{W}$. The platoon formation time depends on how many CAVs a CAV needs to wait to form a platoon with size s. The more CAVs with the same E–E pair entering the corridor, the less waiting time required (Johansson et al., 2021b; Noruzoliaee et al., 2021). For platoon dissolution time, Khoder et al. (2020) showed that with more severe traffic congestion, more time is needed for platoon dissolution because of the queuing delay. It can be seen that the platoon formation time and dissolution time vary in different directions with the traffic flow, with no clear relationship between platoon-related cost and aggregate flow on the E–E pair. In light of this, we simply assume that the platoon-related cost on an E–E pair $\tilde{w} \in \tilde{W}$, $\tau_{\tilde{w}}$, is a small proportion of its free-flow travel time (*i.e.*, $\kappa \sum_{a \in \tilde{w}(:)} t_a^0 \lambda_{CAV}$) as given below.

$$\tau_{\tilde{w}} = \kappa \sum_{a \in \tilde{w}(:)} t_a^0 \lambda_{CAV} + \epsilon,$$

where κ $(0 < \kappa < 1)$ measures the magnitude of the platoon-related cost compared to the free-flow travel time cost on E–E pair $\tilde{w}$. Such consideration is based on the fact that it is not economically practical for CAVs to form platoons if they have to spend more time on platoon formation and dissolution than the free-flow travel time (the lowest travel time). In other words, CAVs will

[2] Some studies consider that the capacity of a road link increases with the CAV penetration ratio on the link (*i.e.*, $\frac{v_a^{CAV}}{v_a}$) (Chen et al., 2017a; Noruzoliaee et al., 2021; Liu and Song, 2019; Wang et al., 2019), based on the assumption that CAVs will perfectly sense and react faster when following other vehicles. However, this may not be true in a mixed-traffic environment, especially with the current CAV technology which is still under development (Li et al., 2020; Ye and Yamamoto, 2018; Do et al., 2019). In fact, it is possible that a CAV needs additional time to react when following an HV, potentially causing traffic flow instability and safety issues (Milanés and Shladover, 2014). Considering the above, it is more sensible to assume that all vehicles maintain a consistent spacing from their followers in mixed traffic.

choose not to form platoons if the platoon-related cost is high. Our motivation stems from Wang et al. (2022) who determined the maximum waiting time for leading vehicles based on their tolerance levels relative to travel time in light traffic (the dissolution time is negligible). To characterize the difference in forming platoons at different times on the corridor, we let ϵ ($\epsilon > 0$) be the inconvenience cost of forming platoons per time.

2.2.3. The definition of PNEMF

On a road network with a given CAV platoonable corridor, we assume that HVs and CAVs make route choices to minimize their respective generalized travel costs following the UE principle. It is reminded that HVs cannot access the CAV platoonable corridor, only routes consisting of non-platoonable links are feasible, whereas CAVs can choose to enter the corridor for platoon formation and, if so, where to enter and exit as well as their respective route choices. To describe the optimal choices adopted by HV and CAV users and obtain the resulting spatial distribution of traffic congestion on a road network with a CAV platoonable corridor at UE, a platoon-embedded network equilibrium with the mixed flow (PNEMF) is developed. The PNEMF is defined as follows.

Definition 1. PNEMF is to find a flow pattern $(\mathbf{h}, \mathbf{x}, \mathbf{v}) \in \Xi$ such that for users of each class, the generalized travel costs of all utilized paths between the same O–D pair are equal and less than or equal to that of those unutilized paths, that is

$$\sum_{a\in A} g_a^{w,CAV}(v_a)\psi_a^r + \sum_{\tilde{w}\in\tilde{W}} g_{\tilde{w}}^{w,CAV}(\mathbf{v})\psi_{\tilde{w}}^r = u^{w,CAV},\ if\ h_r^{w,CAV} > 0, r \in R^{w,CAV}, w \in W, \tag{7}$$

$$\sum_{a\in A} g_a^{w,CAV}(v_a)\psi_a^r + \sum_{\tilde{w}\in\tilde{W}} g_{\tilde{w}}^{w,CAV}(\mathbf{v})\psi_{\tilde{w}}^r \geq u^{w,CAV},\ if\ h_r^{w,CAV} = 0, r \in R^{w,CAV}, w \in W, \tag{8}$$

$$\sum_{a\in A} g_a^{w,HV}(v_a)\psi_a^r = u^{w,HV},\ if\ h_r^{w,HV} > 0, r \in R^{w,HV}, w \in W, \tag{9}$$

$$\sum_{a\in A} g_a^{w,HV}(v_a)\psi_a^r \geq u^{w,HV},\ if\ h_r^{w,HV} = 0, r \in R^{w,HV}, w \in W, \tag{10}$$

where $u^{w,m}$ is the minimum generalized travel cost of O–D pair $w \in W$ for vehicle class $m \in M$. Ξ is the set of feasible flow patterns. Ξ is defined by

$$\sum_{r\in R^{w,m}} h_r^{w,m} = q^{w,m}, \quad \forall w \in W, m \in M, \tag{11}$$

$$h_r^{w,m} \geq 0, \quad \forall r \in R^{w,m}, w \in W, m \in M, \tag{12}$$

$$x_a^{w,m} = \sum_{r\in R^{w,m}} h_r^{w,m}\psi_a^r, \quad \forall a \in A, w \in W, m \in M, \tag{13}$$

$$x_{\tilde{w}}^{w,CAV} = \sum_{r\in R^{w,CAV}} h_r^{w,CAV}\psi_{\tilde{w}}^r, \quad \forall \tilde{w} \in \tilde{W}, w \in W, \tag{14}$$

$$v_a^m = \sum_{w\in W} x_a^{w,m}, \quad \forall a \in A, m \in M, \tag{15}$$

$$v_{\tilde{w}}^{CAV} = \sum_{w\in W} x_{\tilde{w}}^{w,CAV}, \quad \forall \tilde{w} \in \tilde{W}, \tag{16}$$

$$v_a = \sum_{m\in M} v_a^m, \quad \forall a \in A, \tag{17}$$

$$v_a = \sum_{\tilde{w}\in\tilde{W}:\, a\in\tilde{w}(:)} v_{\tilde{w}}^{CAV}, \quad \forall a \in \tilde{A}, \tag{18}$$

where ψ_a^r is a link-path incidence variable. $\psi_a^r = 1$ if a non-platoonable link a is on path r, and $\psi_a^r = 0$ otherwise. $\psi_{\tilde{w}}^r$ is an E–E pair-path incidence variable. $\psi_{\tilde{w}}^r = 1$ if an E–E pair $\tilde{w}$ is on path r, and $\psi_{\tilde{w}}^r = 0$ otherwise. Recall that $q^{w,m}$ denotes the demand of class m for O–D pair w.

Constraint (11) ensures demand conservation, and constraint (12) corresponds to the non-negativity of path flow. Constraints (13)–(14) specify the relationship between path flow and link and E–E pair flow. Specifically, the flow on each non-platoonable link $a \in A$ or E–E pair $\tilde{w} \in \tilde{W}$ between O–D pair $w \in W$ by vehicle class $m \in M$ is the sum of flow on paths that utilize a or $\tilde{w}$. Constraint (15) defines the class-specific aggregate flow on a non-platoonable link. Similarly, constraint (16) shows that the aggregate flow for E–E pair $\tilde{w} \in \tilde{W}$ is the sum of its flow over all O–D pairs. Constraint (17) defines the aggregate flow on a non-platoonable link as the sum of class-specific link flow over vehicle classes. The aggregate flow on a CAV platoonable link is the sum of the flow on that link over all E–E pairs given by constraint (18).

2.3. PNEMF's equivalent variational inequality and solution properties

In this section, we derive an equivalent VI problem for the PNEMF, and then prove the existence and uniqueness of the VI solution.

Proposition 1. *A flow pattern* $(\mathbf{h}^*, \mathbf{x}^*, \mathbf{v}^*) \in \Xi$ *is a PNEMF if and only if it solves the following VI problem*

$$\sum_{a\in A}\sum_{m\in M} g_a^m\left(v_a^*\right)\left(v_a^m - v_a^{m*}\right) + \sum_{\tilde{w}\in\tilde{W}} g_{\tilde{w}}^{CAV}\left(\mathbf{v}^*\right)\left(v_{\tilde{w}}^{CAV} - v_{\tilde{w}}^{CAV*}\right) \geq 0, \quad \forall(\mathbf{h},\mathbf{x},\mathbf{v}) \in \Xi. \tag{PNEMF-VI}$$

The sufficient part can be established by examining the KKT conditions of (PNEMF-VI) and comparing them with (7)–(18), and the necessary part starts with a solution $(\mathbf{h}^*, \mathbf{x}^*, \mathbf{v}^*) \in \Xi$ satisfy (7)–(10), and then (PNEMF-VI) can be derived trivially. Detailed proof can be found in Appendix A.

We now examine the solution properties of the VI problem (PNEMF-VI). The following two propositions state the existence and uniqueness of the solution of (PNEMF-VI), respectively.

Proposition 2 (*Existence*). (PNEMF-VI) *has at least one solution.*

To prove the existence of a flow pattern $(\mathbf{h}, \mathbf{x}, \mathbf{v}) \in \Xi$, we need to show that the feasible set Ξ is a non-empty and bounded polyhedron and the generalized travel cost functions on each non-platoonable link $a \in A$ and E–E pair $\tilde{w} \in \tilde{W}$ are continuous. Please refer to Appendix B for further details.

Proposition 3 (*Uniqueness*). *The solution of aggregate link flows* $\{v_a, a \in A^0\}$ *to the* (PNEMF-VI) *is unique.*

To establish the uniqueness of aggregate link flow in the monetary-based platoon-embedded equilibrium, we begin by converting it to a time-based platoon-embedded equilibrium. Then, we employ a contradiction argument to demonstrate its uniqueness. For complete proof, please refer to Appendix C.

Proposition 4. *At traffic equilibrium, the minimum generalized travel cost* $u^{w,m}$ *between O–D pair* $w \in W$ *by vehicle class* $m \in M$ *is unique, and hourly-based total generalized travel cost* $\sum_{a\in A}\sum_{m\in M} g_a^m(v_a)v_a^m + \sum_{\tilde{w}\in\tilde{W}} g_{\tilde{w}}^{CAV}(\mathbf{v})v_{\tilde{w}}^{CAV}$ *is unique as well.*

Proof. We first show $u^{w,m}$ between each O–D pair $w \in W$ by each vehicle class $m \in M$ is unique. By Proposition 3, we have proved that the aggregate link flow $(v_a)_{a\in A^0}$ for PNEMF is unique. Then, based on the definition of $u^{w,m}$, we have

$$u^{w,m} = \min_{r\in R^{w,m}}\left\{\sum_{a\in A} g_a^m(v_a)\psi_a^r + \sum_{\tilde{w}\in\tilde{W}} g_{\tilde{w}}^{CAV}(\mathbf{v})\psi_{\tilde{w}}^r\right\}, \quad \forall w \in W, m \in M.$$

$u^{w,m}$ is unique because of the uniqueness of $\mathbf{v}$. Then we prove the hourly-based total generalized travel cost is unique as well. Multiplying both sides of (7) and (8) by equilibrium path flow $h_r^{w,CAV}$ and multiplying both sides of (9) and (10) by equilibrium path flow $h_r^{w,HV}$, we have

$$h_r^{w,CAV}\left(\sum_{a\in A} g_a^{w,CAV}(v_a)\psi_a^r + \sum_{\tilde{w}\in\tilde{W}} g_{\tilde{w}}^{w,CAV}(\mathbf{v})\psi_{\tilde{w}}^r\right) = u^{w,CAV}h_r^{w,CAV}, \ if \ h_r^{w,CAV} > 0, r \in R^{w,CAV}, w \in W, \tag{19}$$

$$h_r^{w,CAV}\left(\sum_{a\in A} g_a^{w,CAV}(v_a)\psi_a^r + \sum_{\tilde{w}\in\tilde{W}} g_{\tilde{w}}^{w,CAV}(\mathbf{v})\psi_{\tilde{w}}^r\right) = u^{w,CAV}h_r^{w,CAV}, \ if \ h_r^{w,CAV} = 0, r \in R^{w,CAV}, w \in W, \tag{20}$$

$$h_r^{w,HV}\left(\sum_{a\in A} g_a^{w,HV}(v_a)\psi_a^r\right) = u^{w,HV}h_r^{w,HV}, \ if \ h_r^{w,HV} > 0, r \in R^{w,HV}, w \in W, \tag{21}$$

$$h_r^{w,HV}\left(\sum_{a\in A} g_a^{w,HV}(v_a)\psi_a^r\right) = u^{w,HV}h_r^{w,HV}, \ if \ h_r^{w,HV} = 0, r \in R^{w,HV}, w \in W. \tag{22}$$

By multiplying the inequalities (8) and (10) by those $h_r^{w,CAV}(=0)$ and $h_r^{w,HV}(=0)$, we can derive the equalities (20) and (22). Then by summing up (19) and (20) over all $r \in R^{w,CAV}, w \in W$, and summing up (21) and (22) over all $r \in R^{w,HV}, w \in W$, we have

$$\sum_{w\in W}\sum_{r\in R^{w,CAV}} h_r^{w,CAV}\left(\sum_{a\in A} g_a^{w,CAV}(v_a)\psi_a^r + \sum_{\tilde{w}\in\tilde{W}} g_{\tilde{w}}^{w,CAV}(\mathbf{v})\psi_{\tilde{w}}^r\right) = \sum_{w\in W}\sum_{r\in R^{w,CAV}} u^{w,CAV}h_r^{w,CAV}, \tag{23}$$

$$\sum_{w\in W}\sum_{r\in R^{w,HV}} h_r^{w,HV}\left(\sum_{a\in A} g_a^{w,HV}(v_a)\psi_a^r\right) = \sum_{w\in W}\sum_{r\in R^{w,HV}} u^{w,HV}h_r^{w,HV}. \tag{24}$$

Using (13)–(16) on the left-hand side of (23)–(24), and using (11) on the right-hand side of (23)–(24), the above equations can be expressed as

$$\sum_{a\in A} g_a^{CAV}(v_a)v_a^{CAV} + \sum_{\tilde{w}\in\tilde{W}} g_{\tilde{w}}^{CAV}(\mathbf{v})v_{\tilde{w}}^{CAV} = \sum_{w\in W} u^{w,CAV}q^{w,CAV},$$
$$\sum_{a\in A} g_a^{HV}(v_a)v_a^{HV} = \sum_{w\in W} u^{w,HV}q^{w,HV}.$$

The above two equations can be further simplified as

$$\sum_{a\in A}\sum_{m\in M} g_a^m(v_a)v_a^m + \sum_{\tilde{w}\in\tilde{W}} g_{\tilde{w}}^{CAV}(\mathbf{v})v_{\tilde{w}}^{CAV} = \sum_{w\in W}\sum_{m\in M} u^{w,m}q^{w,m}. \tag{25}$$

Since $(u^{w,m})_{w\in W,m\in M}$ on the right-hand side of (25) is unique, and $q^{w,m}$ is given, hourly-based total generalized travel cost $(\sum_{a\in A}\sum_{m\in M} g_a^m(v_a)v_a^m + \sum_{\tilde{w}\in\tilde{W}} g_{\tilde{w}}^{CAV}(\mathbf{v})v_{\tilde{w}}^{CAV})$ is unique. This completes the proof. □

In summary, at traffic equilibrium, although class-specific non-platoonable link flow $(v_a^m)_{a\in A,m\in M}$, the aggregate flow on E–E pair by CAVs, $(v_{\tilde{w}}^{CAV})_{\tilde{w}\in\tilde{W}}$, path flow $\mathbf{h}$ and link flow $\mathbf{x}$ are generally not unique, the aggregate link flow $(v_a)_{a\in A^0}$, the minimum generalized travel cost $(u^{w,m})_{w\in W,m\in M}$ and hourly-based total generalized travel cost are unique.

2.4. The optimal deployment of an equitable CAV platoonable corridor

After introducing PNEMF to model the route choices of CAV and HV users at the lower level, we now model the problem of finding the optimal deployment of an equitable CAV platoonable corridor as a bi-level program (see Fig. 1). At the upper level, the transportation planner acts as a leader to determine the links to be upgraded to CAV platoonable links and form a corridor to minimize the social cost, which is the weighted average of the sum of the first two components (the upgrade cost and the total generalized travel cost at the target year) and the inequity cost at the target year. For the given CAV platoonable corridor, CAV and HV users act as followers to decide their user-optimal route choices at the lower level. The mathematical formulation for our bi-level program is described as follows:

$$\min_{\mathbf{y}} \quad \pi\Bigg(\underbrace{\sum_{a\in A^0} y_a k_a l_a}_{\text{Upgrade cost}} + \eta\underbrace{\Bigg(\sum_{m\in M}\sum_{a\in A} g_a^m(v_a)v_a^m + \sum_{\tilde{w}\in\tilde{W}} g_{\tilde{w}}^{CAV}(\mathbf{v})v_{\tilde{w}}^{CAV}\Bigg)}_{\substack{\text{Total generalized travel cost}\\ \text{at the target year}}}\Bigg)$$

$$+(1-\pi)\,\eta\underbrace{\Bigg(\sum_{w\in W}\max\left\{0,\left(u^{w,HV}-\bar{u}^{w,HV}\right)\right\}q^{w,HV}\Bigg)}_{\text{Inequity cost at the target year}}$$

$$\text{s.t.} \quad y_a=\{0,1\}, \quad \forall a\in A^0,$$

$$\left|R^{w,m}\right|\geq 1, \quad \forall w\in W, m\in M, \tag{26}$$

$$\text{A sequence } \left(i_1,\ldots,i_{|\tilde{N}|}\right) \text{ of distinct vertices is a simple path,} \tag{27}$$

$$\text{where } |\tilde{N}| = \sum_{i\in N^0}\left(\min\left\{1,\sum_{j\in N^0} y_{(i,j)}+y_{(j,i)}\right\}\right),$$

$$\mathbf{v} \text{ is obtained by solving}$$

$$(7)\text{–}(18),$$

$$\text{given } \tilde{A}=\left\{a\in A^0|y_a=1\right\}, A=\left\{a\in A^0|y_a=0\right\}, \tilde{N}=\left\{i\in N^0|\exists j\in N^0,(i,j)\in\tilde{A}\vee(j,i)\in\tilde{A}\right\},$$

$$\text{and } N=\left\{i\in N^0|\exists j\in N^0,(i,j)\in A\vee(j,i)\in A\right\},$$

$$\text{and } \left(u^{w,HV}\right)_{w\in W} \text{ is the solution of}$$

$$\min_{r\in R^{w,HV}}\left\{\sum_{a\in A} g_a^{HV}(v_a)\psi_a^r\right\}, \quad \forall w\in W, \tag{28}$$

where y_a is a binary decision variable, which decides whether a link a should be upgraded to a CAV platoonable link. y_a takes value 1 if the link a is upgraded to a CAV platoonable link, and takes value 0 if the link a is a non-platoonable link. The first term in the objective function is calculated by $\sum_{a\in A^0} k_a l_a y_a$, where k_a is the upgrade cost per mile, and l_a is the link distance. The second term is the total generalized travel cost at the target year, where $\sum_{m\in M}\sum_{a\in A} g_a^m(v_a)v_a^m + \sum_{\tilde{w}\in\tilde{W}} g_{\tilde{w}}^{CAV}(\mathbf{v})v_{\tilde{w}}^{CAV}$, as we mentioned, represents hourly-based total generalized travel cost, and η denotes the total number of utilized hours at the target year. The last term is calculated by the sum of possibly increased generalized travel cost for each HV, where $u^{w,HV}$ and $\bar{u}^{w,HV}$ represent the HVs' generalized travel costs for the utilized paths on O–D pair w with and without corridor, respectively. Note that each HV with $w\in W$ will be adversely affected by the corridor if the former is larger than the latter, and its inequity cost equals the difference between them; otherwise, no inequity cost exists. $\bar{u}^{w,HV}$ is a solution of $\min_{r\in\bar{R}^{w,HV}}\left\{\sum_{a\in A} g_a^m(\bar{v}_a)\psi_a^r\right\}$, $\forall w\in W$, in which $\bar{\mathbf{v}}$ is obtained by solving (7)– (18) given $\tilde{A}=\emptyset,\tilde{N}=\emptyset,A=A^0,N=N^0$. Again, we multiply $\sum_{w\in W}\max\left\{0,\left(u^{w,HV}-\bar{u}^{w,HV}\right)\right\}q^{w,HV}$ by η to compute the inequity cost at the target year. The weight $\pi\in(0,1)$ is introduced to balance the positive and negative impacts on different road users, and the smaller π, the more concern on the inequity cost.

There are two restrictions for the deployed CAV platoonable corridor. Note that $|R^{w,m}|$ represents the number of paths of O–D pair w by vehicle class m. Constraint (26) demonstrates that each vehicle can find at least one feasible path with the deployed corridor. Constraint (27) defines the deployed corridor should be a sequence of nodes such that links $(i_1,i_2),(i_2,i_3),\ldots,\left(i_{|\tilde{N}|-1},i_{|\tilde{N}|}\right)$ are consecutive CAV platoonable links, and i_j is distinct, where $|\tilde{N}|=\sum_{i\in N^0}\left(\min\left\{1,\sum_{j\in N^0} y_{(i,j)}+y_{(j,i)}\right\}\right)$. To obtain the generalized travel costs of utilized paths between O–D pair $w\in W$ by vehicle class HV with a corridor, we need to solve a lower-level problem given the non-platoonable link set A, the CAV platoonable link set $\tilde{A}$, the set of nodes outside the corridor N, and the set of nodes inside the corridor $\tilde{N}$, and then using (28) to obtain it. Note that the objective function value at the upper level is uniquely

determined on a road network with a given platoonable corridor. To clarify, we separately discuss the uniqueness of the three components in the objective function when a corridor is given. Firstly, the "upgrade cost" could be uniquely determined by A^0 and is therefore unique. Secondly, the "total generalized travel cost" at the target year is also unique because of Proposition 4. Finally, the minimum generalized travel cost $u^{w,HV}$ for the PNEMF between each O–D pair $w \in W$ is also uniquely determined, as demonstrated by Proposition 4. In fact, $\bar{u}^{w,HV}$ is also unique because it represents the minimum generalized travel cost when there is no corridor and therefore we can again apply Proposition 4 with $\tilde{A} = \emptyset, A = A^0, \tilde{N} = \emptyset, N = N^0$.

Remark 1. Note that vehicle platoon may also be enabled outside the corridor using V2V technology, while the impact of vehicle platoon outside the corridor may not significantly affect system-level congestion. Therefore, this study focuses on vehicle platooning with dedicated infrastructure so as to facilitate safer and more stable vehicle platooning for highly concentrated platoon flows. More importantly, providing a CAV platoonable corridor can influence and encourage CAV commuters to use the corridor, so we expect that CAV flows will be more concentrated, resulting in more significant benefits from fuel saving and improved capacity.

3. Solution approach

To address the bi-level program developed in the previous section, we propose a simulated-annealing-based corridor search (SACS) algorithm (see Section 3.1) to find a high-quality CAV platoonable corridor in a desirable amount of time. Specifically, the SACS algorithm starts with an initial solution and then picks a neighborhood solution through a subtle perturbation rule until the stopping criterion is satisfied. To evaluate the solution quality of each iteration, we develop a modified gradient projection (MGP) algorithm (see Section 3.2), which is embedded in the SACS algorithm to quickly solve the PNEMF under the current solution of the upper level.

3.1. Solution algorithm of optimal deployment of a CAV platoonable corridor

To determine the deployment of an equitable CAV platoonable corridor that minimizes the social cost, a subset of links is selected from a road network to be upgraded to CAV platoonable links and form a corridor. In literature, such a problem is categorized as discrete network design problems (DNDPs). Most DNDPs aim to find the optimal link additions from the set of candidate links (*i.e.,* 0–1 decision variables) to minimize the social cost or maximize the social welfare while accounting for road users' route choices. During the past few years, several methods have been proposed to solve DNDPs to global optimality, such as branch-and-bound (Leblanc, 1975), support function concept (Gao et al., 2005), and global optimization method (Wang et al., 2015). However, these methods are often computationally intensive and impractical for solving problems of realistic size. Therefore, modern heuristic/meta-heuristic algorithms, such as simulated annealing (Chen et al., 2017b), genetic algorithms (GAs) (Yin, 2000; Zhang and Yang, 2004; Liu and Song, 2019), partial swam optimization (PSO) (Babazadeh et al., 2011) and ant systems (Poorzahedy and Abulghasemi, 2005; Poorzahedy and Rouhani, 2007), have attracted significant interest. Although these algorithms may not guarantee optimal solutions, they are capable of quickly and effectively finding good solutions.

To find an optimal corridor development while considering the users' route choices, we need to solve a discrete bi-level program with a large solution space, a heuristic solution approach would be desired. The chosen heuristic should satisfy at least three conditions. First, it should be able to avoid being trapped in local optima. Second, it should easily identify a promising solution in the neighborhood of the current solution. Lastly but perhaps most importantly and specifically to this problem, it is ideal not to solve the time-consuming lower-level problem (PNEMF) very often. While there are many promising heuristics that meet these criteria, SA is a standout candidate thanks to its proven track record in handling large solution spaces in reasonable times (Spinellis and Papadopoulos, 2000; Cunha and Sousa, 1999). Indeed, SA is capable of escaping local optima when the temperature is high (Delahaye et al., 2019; Cunha and Sousa, 1999). Also, SA does not depend on restrictive conditions of the model (Kumbharana and Pandey, 2013). In the context of our study, there are two such conditions: first, a qualified corridor consists of a sequence of connected CAV platoonable links without sub-cycles; second, a qualified corridor should not prevent HVs from discovering feasible paths. Under SA, these two considerations can be easily incorporated when generating neighboring solutions. Furthermore, each iteration of SA requires solving the lower-level problem just once. We however, by no means, suggest that the other heuristics cannot be used. Therefore, we develop a simulated-annealing-based corridor search (SACS) algorithm based on the simulated annealing (SA) algorithm (Metropolis et al., 1953; Kirkpatrick et al., 1983; Černỳ, 1985).

The SA algorithm is inspired by the heating and cooling phenomenon of solid materials. Annealing is a process, in which a solid at a high temperature will be transformed into crystalline state at a low temperature by lowering the temperature gradually (Metropolis et al., 1953). Accordingly, our SACS algorithm is developed based on its recent implementations conducted by Zockaie et al. (2016), Ghamami et al. (2016) and Zockaie et al. (2018). The flowchart in Fig. 5 illustrates the procedures of the SACS algorithm. There are two main steps for the SACS algorithm. The first step is searching from the feasible set to find an initial solution and then moving to a neighboring solution. The second step is to compare the objective function value of the current and new solutions to decide whether to accept a new solution with a probability based on the difference. The probability gradually decreases as the solution procedure proceeds.

Specifically, to obtain an initial solution, we solve a lower-level problem without a corridor to obtain $\mathbf{v}$ and then weigh all links based on the CAV-specific aggregate link flow. The initial solution can be found by randomly picking a link based on the weight. To effectively obtain a decent neighboring feasible solution, we specially design a perturbation rule by upgrading a link to a CAV

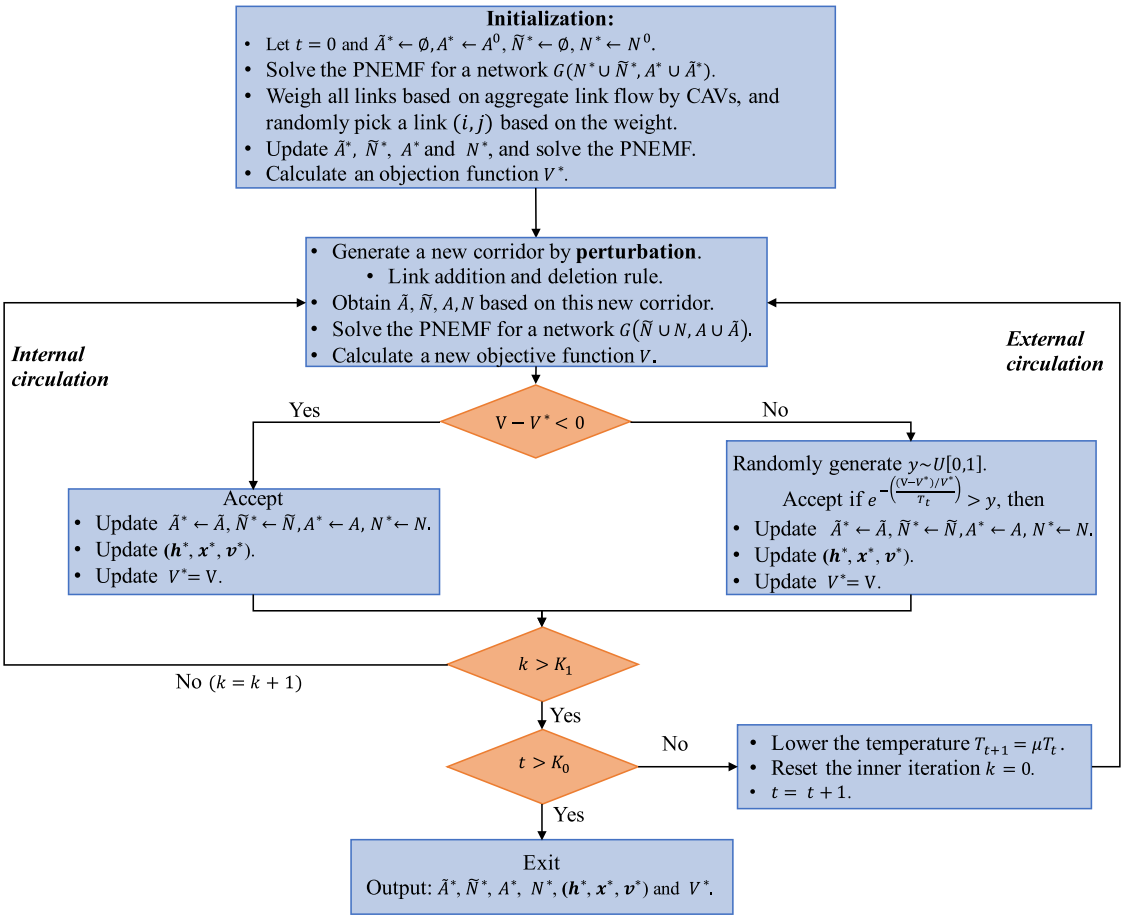

Fig. 5. A flowchart of the SACS algorithm.

platoonable link or downgrading a CAV platoonable link to a non-platoonable link. The details of link addition and deletion rules are described below.

Rule 1 (Link Addition): First, identify all candidate CAV platoonable links that can be appended to the existing corridor: a link (i,j) or (j,i) can be a candidate CAV platoonable link if it connects a candidate non-platoonable node i with a CAV platoonable node j (either at the beginning or at the end of the existing corridor). Then, the algorithm checks the feasibility of the candidate CAV platoonable links: a link if added should not make the CAV platoonable corridor a cycle and stop HVs from finding feasible paths. Finally, weigh all the feasible candidate CAV platoonable links based on the aggregate link flow by CAVs. The link with the largest flow will be most likely to be selected in the next iteration.

Rule 2 (Link Deletion): Identify all candidate CAV platoonable links that can be removed: a link (i,j) or (j,i) is considered to be a candidate CAV platoonable link if the node i is at the beginning or the end of the corridor. Then weigh the candidate CAV platoonable links based on the inversion of aggregate link flow by CAVs. The link with the smallest flow will be most likely to be selected in the next iteration.

We then let the current objective function value be V^*, and the objective function value of neighboring solution be V. If $V \le V^*$, the neighboring solution will be accepted with certainty. Otherwise, the neighboring solution will be accepted with probability $e^{-\left(\frac{(V-V^*)/V^*}{T_t}\right)}$, where T_t represents the controlled temperature at time t. Note that the probability $e^{-\left(\frac{(V-V^*)/V^*}{T_t}\right)}$ gradually decreases with the decreased temperature T_t. Eventually, at a low temperature, the algorithm can only proceed with a solution that strictly dominates the previous one.

The pseudo-code of SACS is presented in Algorithm 1. Four implementation remarks are worth mentioning. First, regarding the perturbation process from line 11 to line 26 at Algorithm 1, when $y \ge 0.5$, it is possible that a feasible candidate CAV platoonable link (i,j) or (j,i) cannot be found when there is no preceding node of its starting node j and succeeding node of the end node j at the current corridor. In this case, Rule 2 will be used to delete a link. Moreover, if the current CAV platoonable corridor is empty, Rule 1 is no longer applicable, and we use the initialization method to randomly pick a link as the initial corridor. When $y < 0.5$, if the current CAV platoonable corridor is empty, we also utilize the initialization method to add a link as the corridor. For other cases, we follow Rule 1 and Rule 2 to decide the perturbation process. Second, the external iteration number K_0 and internal

Algorithm 1 *Simulated-Annealing-Based Corridor Search Algorithm*

Inputs: The maximum number of external iterations K_0, the maximum number of inner iterations K_1, the initial temperature T_0, the temperature reduction parameter μ, the road network topology.
Initialization: $\tilde{A}^* \leftarrow \emptyset$, $\tilde{N}^* \leftarrow \emptyset$, $A^* \leftarrow A^0$, $N^* \leftarrow N^0$.
Solve the lower-level problem for the network $G(N^* \cup \tilde{N}^*, A^* \cup \tilde{A}^*)$ corridor using Algorithm 2.
Weigh all links based on the aggregate link flow of CAV, v_a^{CAV}, and then randomly pick a link (i, j) based on the weight.
update $\tilde{A}^* \leftarrow \tilde{A}^* \cup \{(i,j)\}$, $\tilde{N}^* \leftarrow \tilde{N}^* \cup \{i,j\}$, $A^* \leftarrow A^* \backslash \{(i,j)\}$, and $N^* \leftarrow N^* \backslash \{k \in \{i,j\} : \forall l \in N^*, (k,l) \notin A^* \cap (l,k) \notin A^*\}$.
Solve the lower-level problem for the network $G(N^* \cup \tilde{N}^*, A^* \cup \tilde{A}^*)$ using Algorithm 2 to obtain the current solutions $(\mathbf{h}^*, \mathbf{x}^*, \mathbf{v}^*)$, and compute the current objective function value V^*.
Set $t = 0$.
while $t < K_0$ **do**
    Set the inner iteration counter $k = 0$.
    while $k < K_1$ **do**
        Randomly generate $y \sim U[0, 1]$
        if $y \geq 0.5$ **then**
            if $\tilde{A}^* = \emptyset$ **then**
                Randomly pick a link (i, j) as a corridor.
            else if a link can be found by Rule 1 **then**
                Add one link (i, j) using Rule 1.
            else
                Remove one link (i, j) using Rule 2.
            end if
        else
            if $\tilde{A}^* = \emptyset$ **then**
                Randomly pick a link (i, j) based on the method for the corridor initialization.
            else
                Remove one link (i, j) using Rule 2.
            end if
        end if
        update $\tilde{A} \leftarrow \tilde{A}^* \cup \{(i,j)\}$, $\tilde{N} \leftarrow \tilde{N}^* \cup \{i,j\}$, $A \leftarrow A^* \backslash \{(i,j)\}$, and $N \leftarrow N^* \backslash \{k \in \{i,j\} : \forall l \in N^*, (k,l) \notin A^* \cap (l,k) \notin A^*\}$.
        Solving the lower-level PNEMF for the network $G(N \cup \tilde{N}, A \cup \tilde{A})$ using Algorithm 2.
        Obtain the objective function value V associated with the perturbed solutions.
        Randomly generate $y \sim U[0, 1]$.
        if $V < V^*$ **then**
            Accept and update V^*, and $\tilde{A}^*$, $\tilde{N}^*$, A^*, N^*, and $(\mathbf{h}^*, \mathbf{x}^*, \mathbf{v}^*)$ based on perturbed solutions.
        else if $V \geq V^*$ and $e^{-\left(\frac{(V-V^*)/V^*}{T_t}\right)} > y$ **then**
            Accept and update V^*, and $\tilde{A}^*$, $\tilde{N}^*$, A^*, N^*, and $(\mathbf{h}^*, \mathbf{x}^*, \mathbf{v}^*)$ based on perturbed solutions.
        else
            Discard the perturbed solutions.
        end if
        Set $k = k + 1$.
    end while
    Set $T_{t+1} = \mu T_t$, and $t = t + 1$.
end while
Outputs: The objective function value V^*, the equilibrium solution $(\mathbf{h}^*, \mathbf{x}^*, \mathbf{v}^*)$, the set for CAV platoonable link $\tilde{A}^*$, the set for CAV platoonable node $\tilde{N}^*$, the set for non-platoonable link A^*, and the set non-platoonable node N^*.

iteration number K_1 are chosen based on our sensitivity analysis, whose details can be found in Section 4.3. Following Zockaie et al. (2016), Ghamami et al. (2016), Zockaie et al. (2018), we assume that the initial temperature T_0 is 0.05, and adopt a linear temperature reduction function and let μ be 0.85. Thirdly, Algorithm 1 is designed to find an equitable CAV platoonable corridor, which, in fact, can also be utilized to find multiple corridors sequentially. Finally, the corridor we considered in this study does not have sub-cycles. The reasons are two-fold. From the practical perspective, the expressways in some countries (*e.g.*, Singapore) have no sub-cycles, and hence the corridor if deployed should not have sub-cycles as well. Moreover, a zone (*i.e.,* may have sub-cycles) may not be superior to the defined corridor. Later, we will show a scenario in which our corridor performs much better than a zone.

3.2. Solution algorithm for PNEMF

A basic assumption of the traditional traffic assignment problem is additivity (*i.e.,* the route cost is simply the sum of the costs on the utilized links on that route), but our PNEMF is nonadditive because the platoon-related cost is defined on E–E pairs. Under this

assumption, the traditional link-based algorithms, such as the Frank–Wolfe algorithm, may not be able to solve our PNEMF. In this study, we employ a path-based algorithm to address our PNEMF. A key benefit of path-based algorithms is to monitor path flows. By doing this, we can analyze how the deployed corridor impacts vehicle routing choices and the subsequent geographic distribution of traffic congestion. Also, these path flow patterns can be directly utilized as a reference required in sensitivity analysis (Tobin and Friesz, 1988).

The gradient projection (GP) algorithm, as a well-known path-based method, has been demonstrated to successfully solve traditional traffic assignment problems. Earlier studies by Jayakrishnan et al. (1994) as well as Chen et al. (2002) on the GP algorithm scale the search direction with the diagonal inverse Hessian matrix and assume a unity step size for each iteration. Their empirical studies indicate that a near-optimal solution can be swiftly attained (*i.e.,* 0.001). However, the GP algorithm may face challenges in achieving highly precise solutions (*i.e.*, 1e−10), which may be partly attributable to the unity step size (Perederieieva et al., 2015; Chen et al., 2012). Thus, the careful selection of the step size becomes crucial to reach highly accurate UE solutions. In this study, we develop a modified gradient projection (MGP) algorithm with adaptive step size, to solve our PNEMF. MGP can find the UE by tracking the paths that users of vehicle class $m \in M$ on O–D pair $w \in W$ actually use. We denote the utilized path set as $\hat{R}^{w,m} = \{r | h_r^{w,m} > 0, r \in R^{w,m}\}$. Then a rough description of MGP can be described as four steps.

Step 1 Initialization

$\hat{R}^{w,m} \leftarrow \emptyset$ for all O–D pairs and all vehicle classes. Assume $\mathbf{x}^k$ and $\mathbf{v}^k$ as $\mathbf{0}$, where k represents the iteration number, and $k = 0$ for initialization.

Step 2 Finding a shortest path

Find the path r^* with the lowest generalized travel cost between O–D pair w for vehicle class m, and add it to $\hat{R}^{w,m}$ if it is not already used. For CAVs, the feasible path set $R^{w,CAV}$ for each O–D pair $w \in W$ can be found on the network $G(N \cup \tilde{N}, A \cup \tilde{W})$, and r^* can be found based on the following

$$r^* \in \underset{r \in R^{w,CAV}}{\arg\min} \left(\sum_{a \in A} g_a^{CAV}(v_a^k) \psi_a^r + \sum_{\tilde{w} \in \tilde{W}} g_{\tilde{w}}^{CAV}(\mathbf{v}^k) \psi_{\tilde{w}}^r \right).$$

For simplification, we denote $\sum_{a \in A} g_a^{w,CAV}(v_a^k) \psi_a^r + \sum_{\tilde{w} \in \tilde{W}} g_{\tilde{w}}^{w,CAV}(\mathbf{v}^k) \psi_{\tilde{w}}^r$ as $U_r^{w,CAV}$, and then $U_{r^*}^{w,CAV}$ represents the minimal generalized travel cost between O–D pair w for CAVs.

Regarding HVs, since the platoonable corridor is inaccessible by HVs, the feasible path set $R^{w,HV}$ for each O–D pair $w \in W$ can be found on the network $G(N, A)$. r^* can be found based on the following

$$r^* \in \underset{r \in R^{w,HV}}{\arg\min} \left(\sum_{a \in A} g_a^{HV}(v_a^k) \psi_a^r \right).$$

For simplification, we denote $\sum_{a \in A} g_a^{w,HV}(v_a^k) \psi_a^r$ as $U_r^{w,HV}$, and then $U_{r^*}^{w,HV}$ represents the minimal generalized travel cost between O–D pair w for HVs.

Step 3 Flow shifting

For each O–D pair w and each vehicle class m, shift the flows among paths to get closer to the equilibrium and then update $\mathbf{x}^k$ and $\mathbf{v}^k$.

Step 4 Convergence checking

Drop paths from $\hat{R}^{w,m}$ if they are no longer used (*i.e.,* $h_r^{w,m} = 0$), and let $k \leftarrow k + 1$ and return to Step 2 unless the relative gap (RG) is sufficiently small. RG is defined as:

$$RG = \frac{\sum_{w \in W} \sum_{m \in M} \sum_{r \in \hat{R}^{w,m}} h_r^{w,m} U_r^{w,m}}{\sum_{w \in W} \sum_{m \in M} U_{r^*}^{w,m} q^{w,m}} - 1.$$

Remark 2. Finding the shortest path for each O–D pair $w \in W$ and each vehicle class $m \in M$ in a network with the deployed corridor proceeds in three steps. In the first step, identify the set of E–E pairs $\tilde{W}$ based on the E–E pair definition in Section 2.2.1, and the set of non-platoonable links A. In the second step, construct a graph $G(N \cup \tilde{N}, A \cup \tilde{W})$ for CAVs or a graph $G(N, A)$ for HVs, and assign generalized travel costs to each link $a \in A$ and/or each E–E pair $\tilde{w} \in \tilde{W}$. In the third step, find the shortest path and the associated cost for each O–D pair $w \in W$ and each vehicle class $m \in M$ using the `dijkstra_path` and `dijkstra_path_length` functions provided by the Python package NetworkX.

For the sake of completeness, the pseudo-code of the MGP is given in Algorithm 2.

Algorithm 2 *A Modified Gradient Projection Algorithm*

Inputs: Network topology $G = (N \cup \tilde{N}, A \cup \tilde{A})$, demand $(q^{w,m})_{w\in W, m\in M}$, the E–E pair set $\tilde{W}$, the maximum number of iterations K_0, an acceptable threshold T_1 of RG, and the step size α.
Initialize: $\hat{R}^{w,m} \leftarrow \emptyset\ \forall w \in W, m \in M$.
  Set $k = 0$, and let $\mathbf{x}^k$ and $\mathbf{v}^k$ as $\mathbf{0}$.
  Compute $g_a^m(v_a^k), \forall a \in A,\ m \in M$ and $g_{\tilde{w}}^{CAV}(\mathbf{v}^k), \forall \tilde{w} \in \tilde{W}$.
while $k \le K_0$ or $RG > T_1$ **do**
  for $w \in W$ **do**
    for $m \in M$ **do**
      Find a path r^* with the lowest path cost $U_{r^*}^{w,m}$.
      Add r^* to $\hat{R}^{w,m}$ if $r^* \notin \hat{R}^{w,m}$.
      if $k = 0$ **then**:
        Let $h_{r^*}^{w,m} = q^{w,m}$.
      else
        Shift Flows:
        for $i \in \hat{R}^{w,m} \backslash r^*$ **do**
          Compute the generalized travel cost $U_i^{w,m}$ for path i.
          The flow on path i is updated by $h_i^{w,m} \leftarrow h_i^{w,m} - \frac{\phi_k^{w,m}}{s_i^k}\left(U_i^{w,m} - U_{r^*}^{w,m}\right)$,
          where $s_i^k = \left(\sum_{a\in A_1^0} \frac{\mathrm{d}t_a(v_a)}{\mathrm{d}v_a}\right)\lambda_m$, and A_1^0 represents a link set utilized by either path i
          or r^*, but not on both. $\phi_k^{w,m}$ is a scalar step-size for O–D pair $w \in W$ by vehicle class
          $m \in M$ at k^{th} iteration.
        end for
        $h_{r^*}^{w,m} \leftarrow q^{w,m} - \sum_{i\in\hat{R}^{w,m}\backslash r^*} h_i^{w,m}$.
      end if
      Update $(\mathbf{x}^k, \mathbf{v}^k)$.
      Update $g_a^m(v_a^k), \forall a \in A, m \in M$, and $g_{\tilde{w}}^{CAV}(\mathbf{v}^k), \forall \tilde{w} \in \tilde{W}$.
      Drop Path: Drop path r from $\hat{R}^{w,m}$ if $h_r^{w,m} = 0,\ \forall r \in \hat{R}^{w,m}$.
    end for
  end for
  Compute RG.
  if $RG > T_1$ **then**
    Set $k = k + 1$.
  else
    Set $\mathbf{h}^* = \mathbf{h}$, $\mathbf{x}^* = \mathbf{x}^k$, and $\mathbf{v}^* = \mathbf{v}^k$.
    Break.
  end if
end while
Outputs: the solution of PNEMF under the given corridor $(\mathbf{h}^*, \mathbf{x}^*, \mathbf{v}^*)$.

To find an adaptive step size for our PNEMF, we first follow the steps in Section 3.2 of Sheffi (1985) and interpret the equilibrium conditions as the optimality conditions of the following minimization:

$$\min V(\mathbf{v}) = \sum_{a\in A\cup\tilde{A}} \int_0^{v_a} t_a(\omega)d(\omega) + \sum_{a\in A}\sum_{m\in M} \frac{1}{\lambda_m} f_a^m v_a^m + \sum_{a\in\tilde{A}} f_a^{CAV} v_a \frac{1}{\lambda_{CAV}} + \sum_{\tilde{w}\in\tilde{W}} \frac{1}{\lambda_{CAV}} \tau_{\tilde{w}} v_{\tilde{w}}^{CAV}$$
$$s.t.\ (11)\text{–}(18). \tag{29}$$

The corresponding KKT conditions are illustrated in Appendix D, which are necessary and sufficient as long as all t_a's are increasing.

Then, a line search method can be used to determine a step size $\phi_k^{w,m}$ along the given descent direction. The descent direction is defined in terms of link flows and E–E pair flows $\Delta\mathbf{v} = ((\Delta v_a)_{a\in A\cup\tilde{A}}, (\Delta v_a^m)_{a\in A\cup\tilde{A}}, (\Delta v_{\tilde{w}}^{CAV})_{\tilde{w}\in\tilde{W}})$. To determine the step size $\phi_k^{w,m}$, we can solve the following optimization problem

$$\begin{aligned}
\min\quad & V(\mathbf{v}^{k-1} + \Delta\mathbf{v}\phi_k^{w,m}) = \sum_{a\in A\cup\tilde{A}} \int_0^{v_a^{k-1} + \phi_k^{w,m}\Delta v_a} t_a(\omega)d(\omega) + \sum_{\tilde{w}\in\tilde{W}} \frac{1}{\lambda_{CAV}} \tau_{\tilde{w}} \left(v_{\tilde{w}}^{CAV,k-1} + \left(1_{m=CAV}\phi_k^{w,m}\Delta v_{\tilde{w}}^m\right)\right) \\
& + \sum_{a\in A} \left(\frac{1}{\lambda_{CAV}} f_a^{CAV} \left(v_a^{CAV,k-1} + 1_{m=CAV}\phi_k^{w,m}\Delta v_a^m\right) + \frac{1}{\lambda_{HV}} f_a^{HV} \left(v_a^{HV,k-1} + (1_{m=HV})\phi_k^{w,m}\Delta v_a^m\right) \right) \\
& + \sum_{a\in\tilde{A}} \frac{1}{\lambda_{CAV}} f_a^{CAV} \left(v_a^{k-1} + 1_{m=CAV}\phi_k^{w,m}\Delta v_a^m\right) \\
\text{s.t.}\quad & 0 \le \phi_k^{w,m} \le \bar{\phi}_k^{w,m},
\end{aligned}$$

where $\Delta v_a = \Delta v_a^m = \sum_{i\in\hat{R}^{w,m}} \Delta h_i^{w,m}\psi_a^i \quad \forall a \in A \cup \tilde{A}$, in which $\Delta h_i^{w,m} = -\frac{1}{s_i^k}(U_i^{w,m} - U_{r^*}^{w,m}) \quad \forall i \in \hat{R}^{w,m}\backslash r^*$ and $\Delta h_{r^*}^{w,m} = -\left(\sum_{i\in\hat{R}^{w,m}\backslash r^*} \Delta h_i^{w,m}\right)$. Similarly, $\Delta v_{\tilde{w}}^m = 1_{m=CAV}\left(\sum_{i\in\hat{R}^{w,m}} \Delta h_i^{w,m}\psi_{\tilde{w}}^i\right) \quad \forall \tilde{w} \in \tilde{W}$, and $1_{m=CAV}$ is an indicator function, and it equals 1 if $m = CAV$, and 0 if $m = HV$. The reason why we make such a projection from shifted path flow to the flow on links and E–E pairs is that our MGP is a path-based algorithm. $\bar{\phi}_k^{w,m}$ represents the upper bound of the step size, and we set $\bar{\phi}_k^{w,m} = \min_{i\in\hat{R}^{w,m}}\left(-\frac{h_i^{w,m}}{\Delta h_i^{w,m}} | \Delta h_i^{w,m} < 0\right)$ to guarantee that those non-shortest paths whose flows after shifting are nonnegative (*i.e.*, $h_i^{w,m} + \phi_k^{w,m}\Delta h_i^{w,m} \geq 0 \quad \forall i \in \hat{R}^{w,m}\backslash r^*$). Note that $\mathbf{v}^{k-1}$ represents aggregate flow on links and E–E pairs on the $(k-1)^{th}$ iteration.

To solve the above optimization problem, we follow (Perederieieva et al., 2015) to determine the largest step size $\phi_k^{w,m} = z^r$ for any non-negative integer r, such that the directional derivative of the above objective function is negative. The underlying motivation is to find a step size that reduces the value of the objective function, while it may not necessarily minimize the objective function.

$$\frac{\partial V(\mathbf{v}^{k-1} + \Delta\mathbf{v}\phi_k^{w,m})}{\partial \phi_k^{w,m}} = \sum_{a\in A\cup\tilde{A}} \left(t_a(v_a^{k-1} + \phi_k^{w,m}\Delta v_a)\Delta v_a\right) + 1_{m=CAV}\left(\sum_{\tilde{w}\in\tilde{W}} \frac{1}{\lambda_{CAV}}\tau_{\tilde{w}}\Delta v_{\tilde{w}}^m + \sum_{a\in A\cup\tilde{A}} \frac{1}{\lambda_{CAV}} f_a^{CAV}\Delta v_a^m\right)$$
$$+1_{m=HV}\left(\sum_{a\in A} \frac{1}{\lambda_{HV}} f_a^{HV}\Delta v_a^m\right).$$

The decrement z is set to 0.5 as suggested in Gentile (2014).

4. Numerical analysis

In this section, numerical analysis is conducted to examine the proposed bi-level program and SACS algorithm. In Section 4.1, we investigate the effect of the CAV market penetration ratio and the degree of planner's concern about equity on the deployment of a CAV platoonable corridor on the Nguyen–Dupuis network. Section 4.2 applies the SACS algorithm on the Sioux Falls network to investigate the impact of platoon size on the deployment of a CAV platoonable corridor. Section 4.3 investigates the computational efficiency of the SACS algorithm. This includes a comparison between the SACS algorithm and the Brute-force algorithm, an exploration into how the precision level of UE solutions influences corridor deployment decisions, and an evaluation of scalability of the SACS algorithm through application to both Anaheim and Winnipeg networks. Section 4.4 compares the performance of a CAV platoonable zone and corridor. The algorithms are implemented using Python 3.9 and tested on a Windows PC using a 3.60 GHz computer with 16 GB RAM.

4.1. The Nguyen–Dupuis network

The Nguyen–Dupuis (ND) network, as shown in Fig. 6, consists of 13 nodes, 20 links, and two O–D pairs. The length and free-flow travel time of each link are given in Table 14 in Appendix E. The total travel demand between O–D pair $(1,3)$ is 6000 (vehicles/h) and 5000 (vehicles/h) for O–D pair $(4,3)$. C_a is assumed to be 2000 (vehicles/h) for each link $a \in A$ (C_a^0 is also 2000 (vehicles/h) before upgrading to a CAV platoonable link). Let $\gamma = 0.3$ and platoon size $s = 3$, then the capacities on CAV platoonable links can be calculated by Eq. (4). Given the complexities associated with calibrating the default parameters α and β for the BPR function, especially in the absence of real-world data, we follow Zhang and Yang (2004), Wang et al. (2013), and Liu and Song (2019), assuming default parameter values for α and β to be 0.15 and 4, respectively. Following Liu et al. (2021), we set VoTs as $\lambda_{CAV} = 3.75$ ($/h) and $\lambda_{HV} = 7.5$ ($/h). Note that $\lambda_{CAV} < \lambda_{HV}$ since CAV users can devote their in-vehicle time to other activities rather than driving, such as work or entertainment (Van den Berg and Verhoef, 2016). According to the data from U.S. Energy Information Administration, the unit fuel price for HVs is 2.242 ($/gallon),[3] and the fuel economy is 25.3 (miles/gallon).[4] Then $\theta_{HV} = 2.242/25.3 = 0.09$ ($/mile). Compared to HVs, autonomous driving technology enables CAVs to traverse in a fuel-efficient way. Therefore, when CAVs traverse on links outside the CAV platoonable corridor, we follow Berry (2010) and Wadud et al. (2016) to assume $\theta_{CAV} = 0.081$ ($/mile). If a CAV enters the CAV platoonable corridor, the fuel cost can be further reduced because of CAV platooning. Hussein and Rakha (2021) explored how platoon formation influences fuel savings. We set δ based on their findings, and the details can be found in Table 15 in Appendix E. In terms of the platoon-related cost, let $\kappa = 0.02$ and $\epsilon = 1e{-}4$. The link upgrading cost k_a is set as 200000 ($/mile) for each link $a \in \tilde{A}$ (Madadi et al., 2021). To convert the hourly-based generalized travel cost and inequity cost to the annual counterparts, we consider there are eight peak hours per day (*i.e.*, four hours of morning peak and four hours of evening peak), then we have $\eta = 8 \times 30 \times 12 = 1920$ hours. In terms of the preference parameter for the planner, we simply assume $\pi = 0.8$. To ensure that the precision level of the UE does not influence the corridor deployment, we set RG to be 1e−10.

[3] https://www.eia.gov/totalenergy/data/browser/?tbl=T09.04#/?f=A&start=1949&end=2020&charted=10-11

[4] https://www.eia.gov/totalenergy/data/browser/?tbl=T01.08

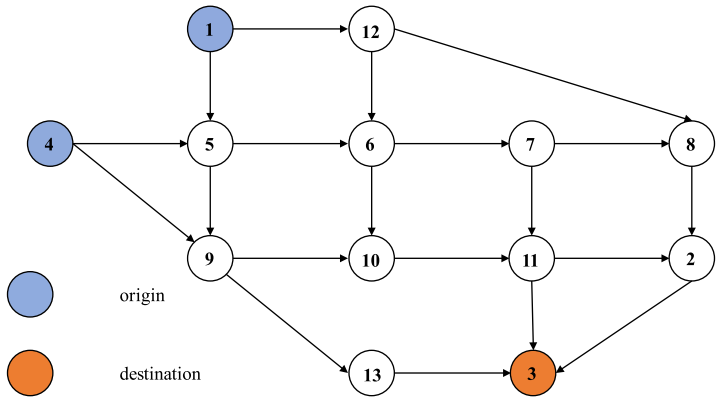

Fig. 6. The Nguyen-Dupuis network.

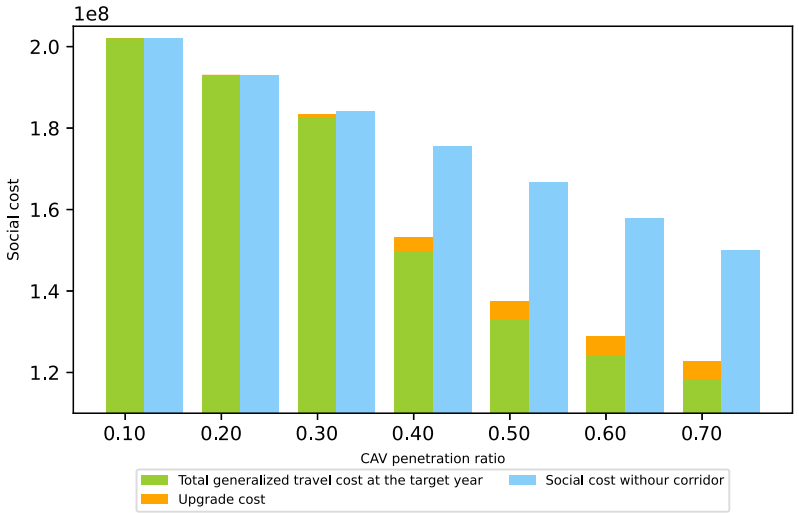

Fig. 7. The social costs for different CAV market penetration ratios.

4.1.1. The effect of CAV market penetration ratio

We consider a range of CAV market penetration ratios for each OD pair, from 10% to 70% with an increment of 10%. In doing so, we examine the impact of the CAV market penetration ratio on the deployment of the equitable CAV platoonable corridor. The demand for CAVs of the O–D pair $w \in W$ can be calculated by multiplying the CAV market penetration ratio with the total travel demand for that specific O–D pair. Then the demand for HVs of the same O–D pair can be derived by subtracting the CAV demand from the total travel demand. Fig. 7 shows the upgrade cost, total generalized travel cost at the target year and the inequity cost at the target year with and without the corridor for different CAV market penetration ratios. It can be seen that the social cost with the deployed corridor is always lower than that without the corridor when the CAV market penetration ratio is not less than 30%, which indicates that the deployment of the CAV platoonable corridor socially benefits the system. That being said, deploying a CAV platoonable corridor is recommended when the CAV market penetration ratio exceeds a threshold (*i.e.,* 30%). Moreover, the deployment of a CAV platoonable corridor is equitable for HVs since there is no associated inequity cost. In other words, the generalized travel costs for HVs do not increase as a result of the deployed corridor. Fig. 8 displays the optimal deployment of the CAV platoonable corridor for different CAV market penetration ratios. The length of the optimal CAV platoonable corridor increases with CAV market penetration ratios as we expect since the infrastructure should be updated gradually to accommodate more CAVs in practice.

We can easily deduce that the reduced social cost is attributed to the decreased total generalized travel cost at the target year when the corridor is deployed. To further explore why deploying a CAV platoonable corridor reduces the total generalized travel cost, Table 2 examines the generalized travel costs of utilized paths for CAVs and HVs respectively when the CAV market penetration ratio is 60%. The generalized travel costs of CAVs for O–D pairs $(1, 3)$ and $(4, 3)$ are significantly reduced by 26.698% and 17.763%, respectively. This quantifies the benefit that CAVs gain from the corridor. Even more intriguing, the generalized travel costs of HVs for O–D pairs $(1, 3)$ and $(4, 3)$ are also significantly reduced by 21.350% and 20.937%, respectively, which implies that traffic

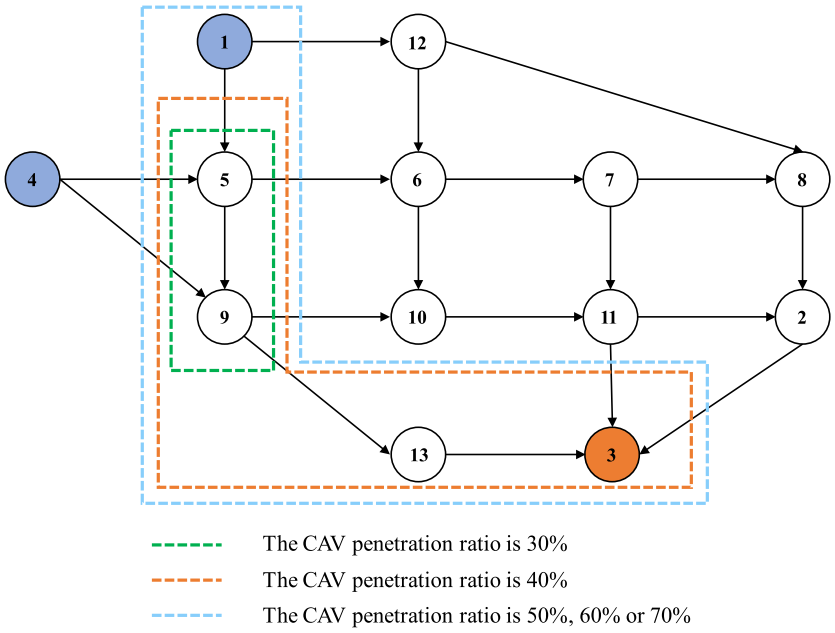

Fig. 8. Optimal CAV corridor deployments at different CAV market penetration ratios.

Table 2
The generalized travel costs of utilized paths with and without the corridor.

O–D pair	Scenario	Generalized travel cost for CAVs ($)	Generalized travel cost for HVs ($)
(1, 3)	With the corridor	5.678	9.714
	Without the corridor	7.746	12.351
(4, 3)	With the corridor	5.949	9.701
	Without the corridor	7.234	12.270

congestion outside the corridor is mitigated due to the deployment of the corridor. Table 3 elaborates on the utilized paths under UE between each O–D pair by each vehicle class. To distinguish CAVs' platoon formation and dissolution behaviors, we demonstrate the utilized paths with a style that every two consecutive nodes are either a non-platoonable link or an E–E pair (the E–E pair is marked in bold). As expected, there is no two or more consecutive E–E pairs appear in CAVs' utilized paths, which is consistent with the setting of the additional cost. Another finding is that the majority of CAVs are attracted by the CAV platoonable corridor and prefer to choose paths with CAV platoonable links. HVs, as a consequence, may not need to compete with CAVs on the remaining paths. For instance, the path $(1, 12, 8, 2, 3)$ previously shared with CAVs when the corridor is not deployed is fully utilized by HVs when the corridor is deployed. In conclusion, the deployment of a CAV platoonable corridor successfully alleviates traffic congestion by reasonably distributing the traffic flow of CAVs and HVs.

4.1.2. The effect of the planner's concern degree on inequity

To well balance the positive and negative impacts of the deployment of a CAV platoonable corridor on CAVs and HVs, we introduce a weightage π to capture the tradeoff between the sum of upgrade cost and total generalized travel cost and the inequity cost in the objective function of the bi-level program. The smaller the π, the more concern of the planner on the inequity cost. This section analyzes the effect of various π on the deployment of the CAV platoonable corridor. The CAV market penetration ratio is set as 30%. Fig. 9 shows that the optimal corridor is $(5, 9)$ when $\pi = \{0.1, 0.2, 0.3, 0.4, 0.5, 0.6, 0.7, 0.8\}$ (see yellow area), and the optimal corridor becomes $(5, 9, 13, 3)$ when $\pi = \{0.9, 1.0\}$ (see green area). It can be interpreted as the planner prefers to deploy a longer CAV platoonable corridor if he/she pays little or even no attention to inequity. In order to compare the performance of the two platoonable corridors, Table 4 displays the social cost and its components for different values of π. Although deploying a corridor $(5, 9, 13, 3)$ can achieve a lower total generalized travel cost, the upgrade and inequity costs are higher than that of deploying the corridor $(5, 9)$, and hence the aggregate performance of the former is not better than that of the latter when $\pi = 0.8$. When $\pi = 0.9$, the inequity cost becomes less significant compared to the case when $\pi = 0.8$, and the sum of the upgrade and total generalized travel costs becomes more meaningful. Hence, a different corridor $(5, 9, 13, 3)$ is preferred. Considering the CAV market penetration ratio is 30%, the planner should pay more attention to equity and choose the corridor $(5, 9)$.

The left-hand side and right-hand side of Fig. 9 also display the utilized paths of HVs for O–D pairs $(1, 3)$ and $(4, 3)$, respectively, when the corridor is $(5, 9, 13, 3)$. HVs cannot utilize the path $(4, 9, 13, 3)$ with this corridor deployment, which is the main reason for

Table 3
Path flow patterns under UE when the CAV market penetration ratio is 60%.

Scenario	O–D pair	Vehicle class	Path	Path flow
With the corridor	(1, 3)	CAV	(**1**, **3**)	3600.000
		HV	(1, 12, 8, 2, 3)	1965.527
			(1, 12, 6, 7, 11, 3)	434.473
	(4, 3)	CAV	(4, **5**, **3**)	2187.751
			(4, 9, 10, 11, 3)	744.174
			(4, **9**, **3**)	68.075
		HV	(4, 5, 6, 7, 11, 3)	1730.459
			(4, 9, 10, 11, 3)	269.541
Without the corridor	(1, 3)	CAV	(1, 5, 9, 13, 3)	2598.111
			(1, 5, 6, 7, 11, 3)	526.317
			(1, 12, 8, 2, 3)	475.572
		HV	(1, 12, 8, 2, 3)	2400.000
	(4, 3)	CAV	(4, 9, 10, 11, 3)	1830.236
			(4, 9, 13, 3)	1169.764
		HV	(4, 5, 6, 7, 11, 3)	1748.312
			(4, 9, 10, 11, 3)	198.705
			(4, 5, 6, 7, 11, 2, 3)	45.928
			(4, 9, 10, 11, 2, 3)	7.055

Table 4
Social costs on the ND network with various cost weightage π.

Scenario	Upgrade cost ($)	Total generalized travel cost ($)	Inequity cost ($)	Social cost ($)
$\pi = 0.8$	1.100e+6	2.281e+8	0.00	1.833e+8
$\pi = 0.9$	4.440e+6	2.236e+8	7.983e+6	2.060e+8

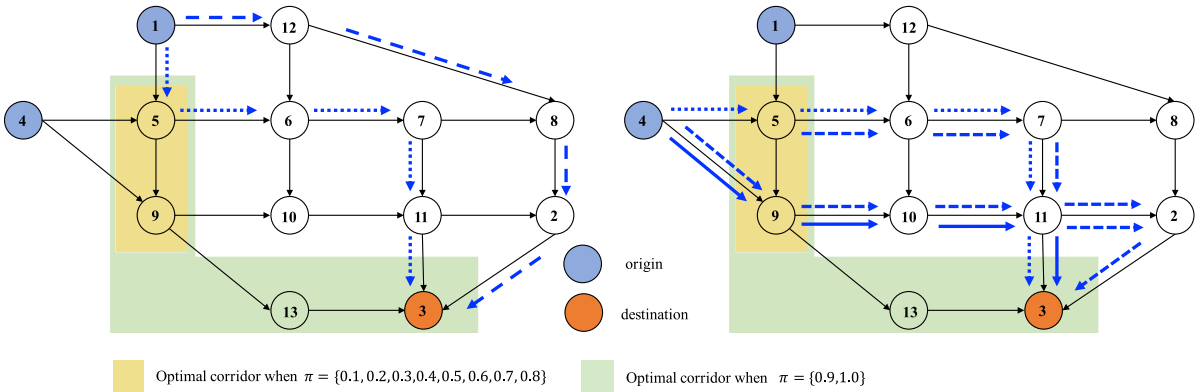

Fig. 9. HV utilized paths for different O–D pairs with the deployed corridor $(5, 9, 13, 3)$.

the incurred inequity cost, while this path is still accessible for HVs if the deployed corridor is $(5, 9)$. We subsequently investigate the path costs utilized by both CAVs and HVs when the corridor is $(5, 9, 13, 3)$. The result demonstrates that the generalized travel costs of utilized paths for CAVs are significantly decreased by more than 31% for both O–D pairs. On the contrary, HVs' generalized travel costs are increased by 4% for both O–D pairs. To conclude, the degree of the planner's concern on equity will influence the deployment of the CAV platoonable corridor, and the inequity issue should be given significant consideration, particularly when the CAV market penetration ratio is low.

4.2. The Sioux Falls network

We further apply the proposed model in a larger-sized network, the Sioux Falls (SF) network (see Fig. 11), to explore the impact of platoon size on the corridor deployment. This network consists of 24 nodes and 76 links. The link characteristics and demand can be found at https://github.com/bstabler/TransportationNetworks/tree/master/SiouxFalls, and we assume the CAV market penetration ratio is 80%. The settings of the remaining parameters are the same as the ND network.

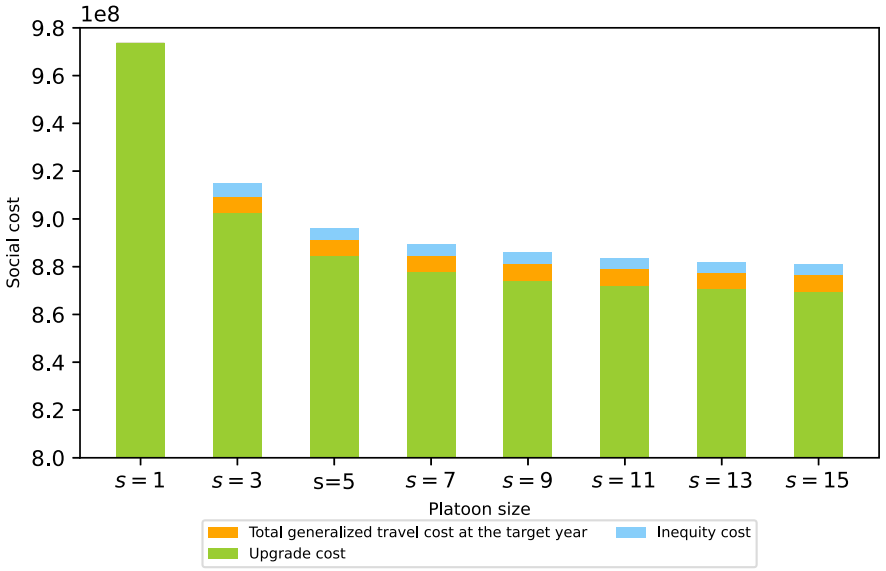

Fig. 10. The social costs for the SF network with different platoon sizes.

Table 5
Reduced proportion of total generalized travel cost with different platoon sizes.

Vehicle class	$s = 3$	$s = 5$	$s = 7$	$s = 9$	$s = 11$	$s = 13$	$s = 15$
CAV	11.996%	13.848%	14.530%	14.955%	15.223%	15.399%	15.518%
HV	−4.464%	−2.593%	−1.899%	−1.727%	−1.601%	−1.527%	−1.478%

4.2.1. The effect of platoon size

This section investigates how the platoon size influences the deployment of CAV platoonable corridor. We consider a range of platoon sizes from three to fifteen. While longer platoons can increase road capacity, they can negatively affect traffic stability (Zhou and Zhu, 2021). This is because longer platoons may reduce lateral maneuverability, making it challenging to merge or split from the platoon (Zhao and Sun, 2013; Liu et al., 2018). In contrast, smaller platoons can facilitate flexible movements such as merging, splitting, or lane changing (Yao et al., 2022). As prior studies have suggested a maximum platoon size range of 10–20 (Liu et al., 2018; Xiao et al., 2018; Robinson et al., 2010), we take the average value and set the maximum allowable platoon size to 15. Using this limit, we investigate corridor design under different platoon sizes for the SF network. The improved link capacity and reduced fuel cost on each CAV platoonable link can be calculated by Eq. (4) and Table 15, respectively.

Fig. 10 illustrates how platoon size affects the social cost and its components. As the platoon size grows, there is a noticeable decline in the social cost. Regarding its components, the upgrade cost remains unchanged, which suggests that the configuration of the deployed corridor remains consistent as the platoon size expands from 3 to 15. Besides, the total generalized travel and inequity costs decrease with the increased platoon size. We also individually compute the reduced proportion of social cost with the deployed corridor compared to that without the corridor for different road users, shown in Table 5. Not surprisingly, CAVs benefit from the deployed corridor as it is dedicated for their use. Besides, the growth rates of the reduced proportion of total generalized travel cost diminish for CAVs as platoon size increases. This is due to the fact that the link capacity and fuel cost on CAV platoon links improve as platoon size increases, but the rate of improvement slows down. Additionally, HVs are adversely impacted by the deployed CAV platoonable corridor since the reduced proportion of total generalized travel cost with the deployed corridor for HVs compared to that without the deployed corridor is negative. However, this negative impact decreases with the increased platoon size, which explains why the inequity cost decreases with the platoon size.

Next, we take a further look at how the link flow changes with and without the CAV platoonable corridor, and we let $s = 3$. As can be seen from Fig. 11, almost all CAV platoonable links witness an increase in traffic flow after deploying the corridor, which could be attributed to the increased capacity and reduced fuel consumption. Moreover, the deployed corridor is (6, 8, 16, 10, 11, 12) (marked in green). To investigate why the corridor deployment is in this manner, we evaluate the demand density among different O–D pairs (see Fig. 12) and discover that O–D pairs (10, 16), (16, 10), and (11, 10) have a high demand density. This suggests that the corridor is strategically positioned in the most congested area to effectively alleviate traffic congestion. Considering HVs bear the increased generalized travel cost, we pick up one O–D pair $(16, 3)$ for further elaboration. The generalized travel costs of utilized paths for these HVs increase from \$5.001 to \$5.374. This occurs because the utilized paths are $(16, 8, 9, 5, 4, 3)$, $(16, 8, 6, 5, 4, 3)$, and $(16, 10, 9, 5, 4, 3)$ when there is no CAV platoonable corridor. However, these three routes become inaccessible when the corridor is deployed, and as a result, the utilized route becomes longer, specifically as $(16, 18, 7, 8, 9, 5, 4, 3)$.

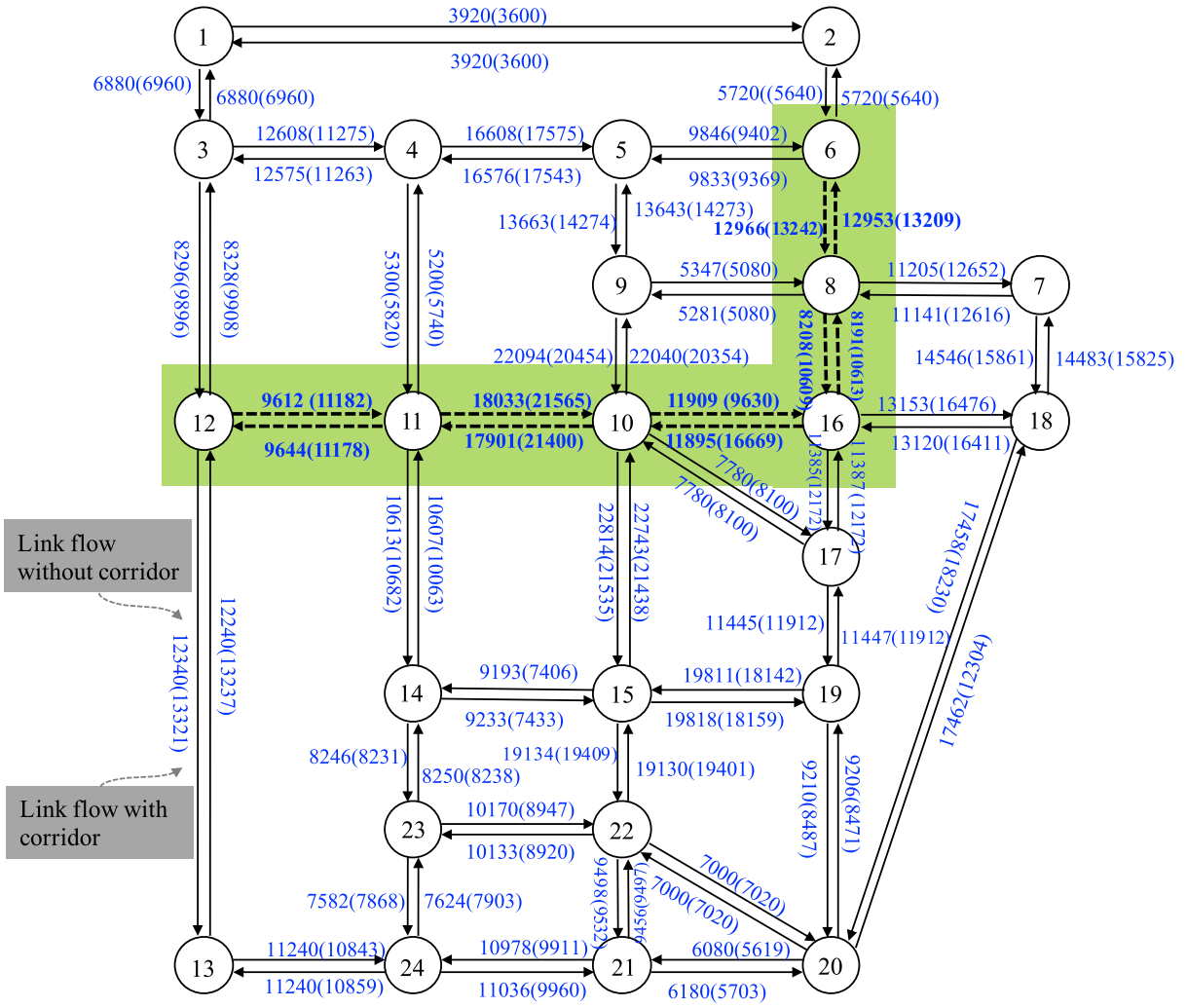

Fig. 11. The aggregate link flow with and without corridor on the SF network.

Furthermore, we compute the fuel cost and travel time cost for each vehicle class across all O–D pairs, as illustrated in Fig. 13, to delve further into how the decreased total generalized travel cost is distributed into travel time cost and fuel cost. In terms of CAVs, the presence of the corridor leads to varying effects on fuel costs, with some O–D pairs experiencing a decrease and others showing an increase. However, the majority of O–D pairs observe a significant reduction in travel time costs. On the other hand, for HVs, the fuel costs across all O–D pairs either remain the same or become even larger compared to the scenario without the corridor. Nevertheless, some HVs benefit from the reduced travel time costs. For example, the travel time cost for HVs with O–D pair $(20, 10)$ notably decreases from \$1074.193 to \$926.918. The increased fuel cost for CAVs can be attributed to their detoured routing to access the corridor, while the increased fuel cost for HVs arises from their inability to utilize links within the corridor. Conversely, the travel time cost for CAVs decreases due to the increased road capacity facilitated by the corridor. Additionally, as CAVs concentrate within the corridor, congestion outside the corridor can be alleviated, which benefits several HVs, resulting in a decrease in their generalized travel cost along the utilized paths.

Last but not least, considering several HVs still suffer a higher generalized travel cost, we propose some potential methods here. One method is to choose a smaller π until the inequity cost disappears. A potential issue is that the deployed CAV platoonable corridor under a smaller π may not significantly improve CAVs' generalized travel costs. An alternative method could entail offering subsidies or compensation to HVs adversely impacted by the existence of the CAV platoonable corridor. This can alleviate the financial burden of increased generalized travel costs for HVs and promote a more equitable distribution of benefits within the transportation system.

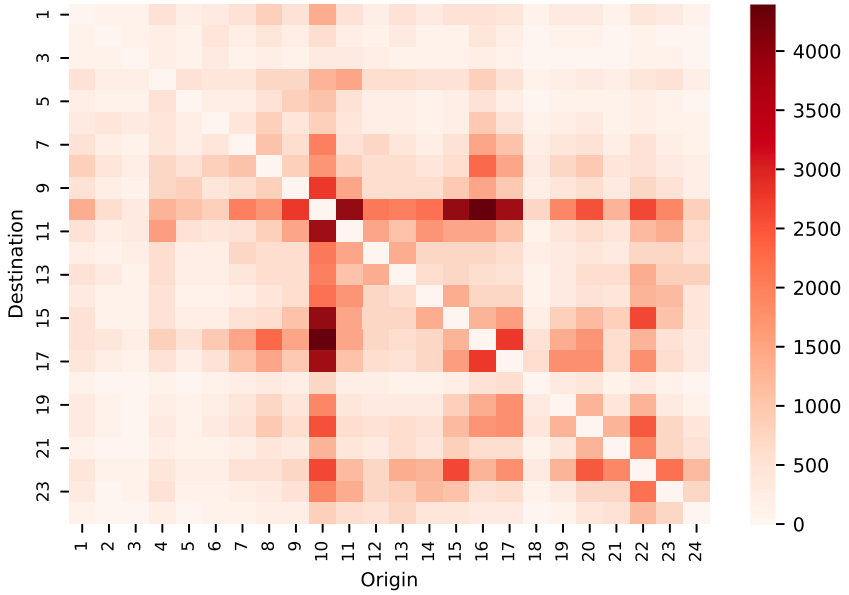

Fig. 12. The demand density between different O–D pairs.

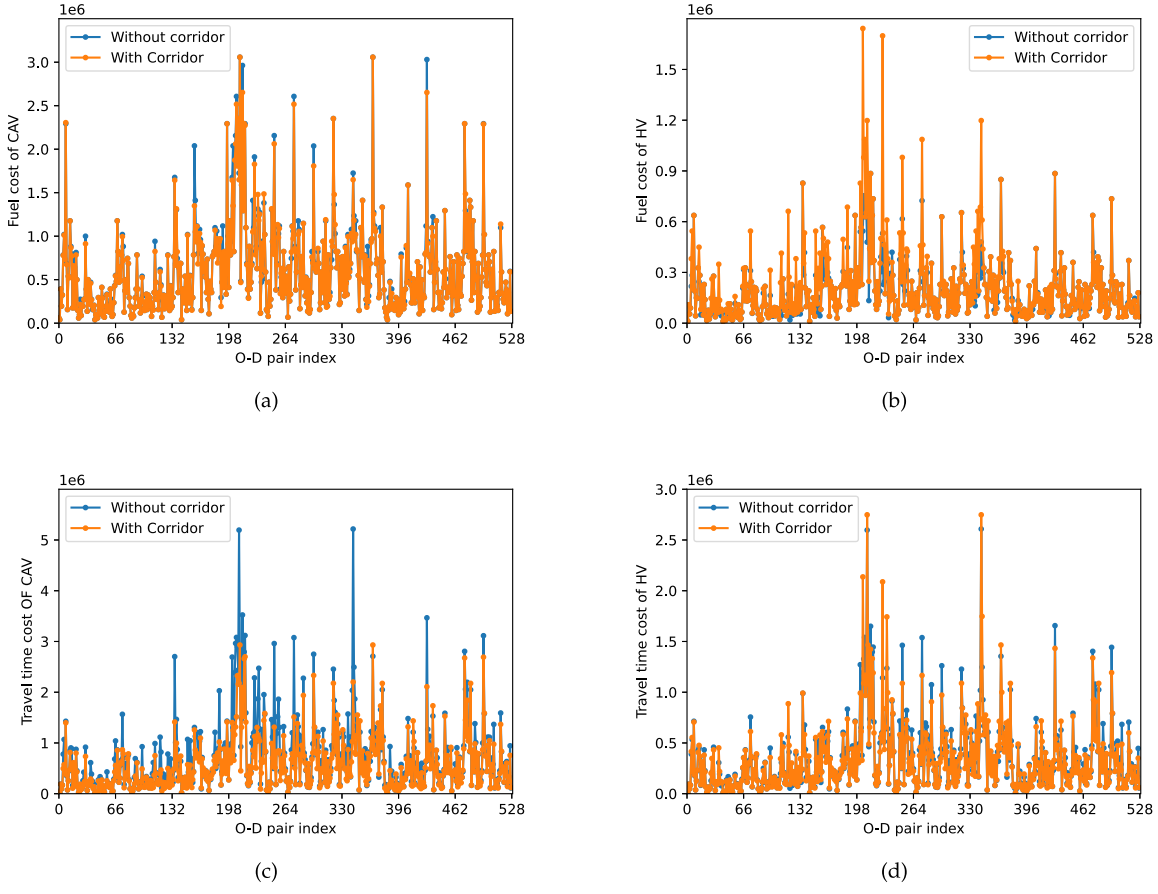

Fig. 13. The travel time cost and fuel cost between each O–D pair for the two vehicle classes.

Table 6
The comparison between SACS and Brute-force algorithms.

Scenario	Methods	Optimal design	Computation time (s)
AV penetration ratio is 70% platoon size $s = 2$	SACS algorithm Brute-force algorithm	(1, 5, 9 ,13, 3) (1, 5 ,9, 1 3, 3)	39.544 325.815
AV penetration ratio is 70% platoon size $s = 15$	SACS algorithm Brute-force algorithm	(1, 5 ,9, 1 3, 3) (1, 5 ,9, 1 3, 3)	10.705 296.300
AV penetration ratio is 30% platoon size $s = 2$	SACS algorithm Brute-force algorithm	(5, 9) (5, 9)	2.202 230.896
AV penetration ratio is 30% platoon size $s = 15$	SACS algorithm Brute-force algorithm	(5, 9) (5, 9)	2.297 228.056

1. $K_0 = 20,\ K_1 = 20$.

Table 7
The impact of different RG on the deployment of a CAV platoonable corridor.

RG	Social cost ($)	Computation time (s)	Corridor
1e−4	914,581,349.004	448.616	(6, 8, 16, 10, 11, 12)
1e−6	914,971,158.994	1596.570	(6, 8 ,16, 10, 11, 12)
1e−8	914,974,796.326	24970.726	(6, 8, 16, 10, 11, 12)
1e−10	914,974,789.601	26035.624	(6, 8 ,16, 10, 11, 12)

1. The maximum number of iterations is 5000 for the lower-level PNEMF.

4.3. Performance of the SACS algorithm

To evaluate the performance of the SACS algorithm, we first compare it with the Brute-force algorithm. Subsequently, considering that varying levels of precision in the lower-level PNEMF could affect corridor deployment decisions at the upper level, we conduct an experiment on the SF network to shed light on this. We finally explore the scalability of the SACS algorithm by applying it to large-scale networks, including the Anaheim and Winnipeg networks.

4.3.1. The comparison between SACS and Brute-force algorithm

We begin by investigating the required number of internal and external iterations for the SACS algorithm. We conduct a comprehensive sensitivity analysis on the SF network to determine the impact of different combinations of internal and external iterations on the optimal objective function value. Through the analysis, we find that the objective function value at the upper level stabilizes after approximately 20 iterations for both internal and external iterations, and no observation suggests employing a larger number of K_0 or K_1 since the CAV platoonable corridor does not change. Considering that increasing the number of iterations significantly escalates the computational cost, we choose $K_0 = 20$ and $K_1 = 20$ for our numerical experiments to strike a balance between computational efficiency and solution quality.

We then proceed to compare the performance of the SACS algorithm with the Brute-force algorithm on the ND network. Table 6 presents the optimal designs and CPU times obtained using both algorithms across different CAV market penetration ratios and platoon sizes. Our objective is to assess the quality of solutions generated by the SACS algorithm. In each case, the SACS algorithm consistently yields optimal corridor designs while maintaining significantly reduced computation time compared to the Brute-force algorithm. This demonstrates the effectiveness of the SACS algorithm in finding equitable CAV platoonable corridor deployments for the ND network.

4.3.2. The impact of the precision level of UE solutions

To investigate how different precision levels of UE solutions affect the deployment of a CAV platoonable corridor, we consider RG can take values of $\{1e{-}4, 1e{-}6, 1e{-}8, 1e{-}10\}$ and evaluate the deployed corridor on the SF network using data from https://github.com/bstabler/Transportationetworks/tree/master/SiouxFalls. We assume an 80% CAV market penetration ratio and a platoon size of three. Table 7 presents the social cost, computation time, and deployed corridor for different RG. Our results show that the value of RG does not affect the deployment of the corridor, suggesting that pursuing high-precision UE solutions is not necessarily advantageous. Please note, in order to highlight the subtle variations in social cost across different precision levels, we do not use the scientific notation method commonly used in other tables to represent social cost.

Finally, to explain why there is a sudden increase in computation time when the relative gap RG is changed from 1e−6 to 1e−8, Fig. 14 demonstrates the detailed iteration results of the MGP algorithm with an adaptative step size on the SF network given the corridor design $(6, 8, 16, 10, 11, 12)$. It can be seen that the algorithm tends to "stall" when the relative gap RG is around 1e−7, and then suddenly experiences a significant performance boost.

Based on the aforementioned arguments, we can see that pursuing high-precision level of UE solutions may not be necessarily significant in our study. We also examine the precision level adopted by the existing literature on network design problems and find that Liu et al. (2021) and Wang et al. (2021) use $RG \in [1e{-}4, 1e{-}6]$. Therefore, to solve our corridor deployment problem, the focus should be on how to use the SACS algorithm to find a high-quality corridor at a reasonable time rather than purely pursuing the

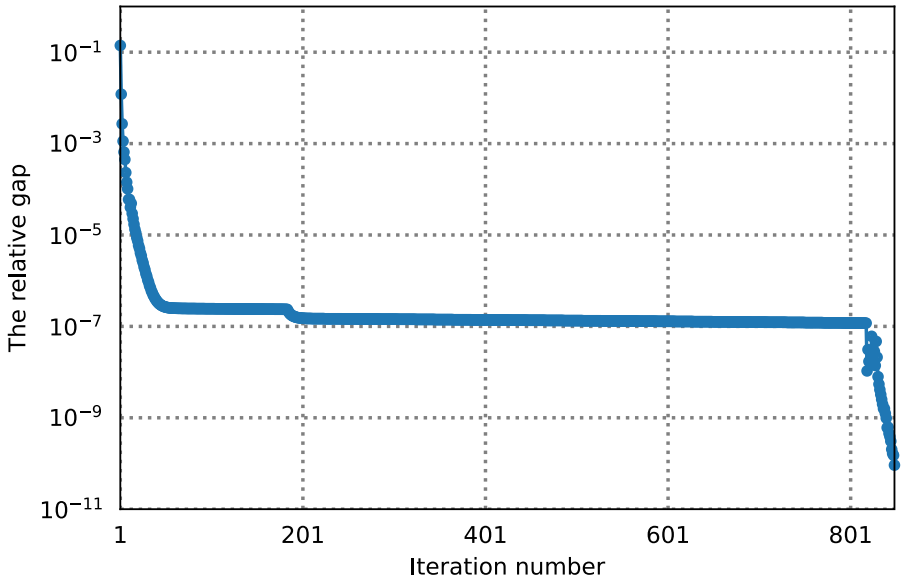

Fig. 14. Computation performance of MGP with adaptive step size.

high-precision of UE solutions without considering its increased computation time on finding the corridor deployment. With this in mind, for large-scale networks, we suggest choosing an acceptable precision level, such as 1e−6, to well balance between accuracy and computational efficiency.

4.3.3. The scalability of SACS algorithm

We first implement the SACS on the Anaheim network. Fig. 15 illustrates the network structure of the Anaheim network. Note that the input parameters for links, including free-flow travel time, link distance, and base link capacity, as well as the O–D pairs and their corresponding demands, can be found at https://github.com/bstabler/TransportationNetworks/tree/master/Anaheim. We assume a CAV market penetration ratio of 60% and a platoon size of three. The other parameter settings are consistent with those of the ND network; see Section 4.1.

Interestingly, when the CAV market penetration ratio is 60%, the deployed corridor on the Anaheim network is $(393, 394)$, which is much shorter than that on the ND network. To understand why, we compare the congestion levels of these two networks by individually calculating the ratio of the number of links whose aggregate link flow v_a exceeds its capacity c_a to the total number of links under equilibrium. Our results show that 75% and 5.8% of links whose aggregate link flow exceeds the corresponding capacity on the ND and Anaheim networks, respectively. This indicates that the Anaheim network is much less congested, which may be one reason why the deployed corridor on the Anaheim network is much shorter than on the ND network. Considering that the network is not congested under this demand, we further experiment with alternative demand levels, at 1.5, 2, 2.5, and 3 times of the base demand level (demand level one), denoted as demand level two, three, four, five, respectively.

Table 8 presents social costs on the Anaheim network for various demand levels. The demand level impacts not only the optimal location of the corridor but also its length. Higher demand levels lead to longer corridors. Another finding from Table 8 is that the proportion of social cost reduction increases with the demand level, indicating the effectiveness of the corridor in mitigating traffic congestion and improving the system efficiency. Thus, it is beneficial to deploy a longer corridor for more congested networks to accommodate more CAVs to form platoons. This strategy will reduce fuel consumption, increase capacity within the corridor, and ultimately alleviate traffic congestion outside the corridor. In addition, Table 9 exhibits the total travel time cost and fuel cost for various vehicle classes with and without the deployed corridor on demand level five. There is a decrease in the travel time cost for both CAVs and HVs, indicating that the corridor helps to mitigate traffic congestion within and outside the corridor. Additionally, the fuel cost for CAVs decreases, while HVs experience a slight increase in fuel cost, which may be attributed to longer distances traveled by HV users to attain the lower travel time cost. Finally, Table 10 reports the computation time taken for various demand levels. It is not surprising that the computation time increases with the demand level, which is consistent with the results reported in Chen et al. (2012).

Next, we implement the SACS algorithm on the Winnipeg network, as depicted in Fig. 16. Please note that network inputs such as free-flow link travel time, link distance, base link capacity, and O–D pair demand are obtained from https://github.com/bstabler/TransportationNetworks/tree/master/Winnipeg-Asymmetric. Also, following this online data, the values for α and β in the BPR function for link travel time are set to be 0.1 and 1.5. We assume a CAV market penetration ratio of 60% and a platoon size of three. Considering the increased network size and O–D pairs of the Winnipeg network, we opt to use an acceptable precision level, with RG = 1e−6. The values for other parameters remain the same as those for the ND network.

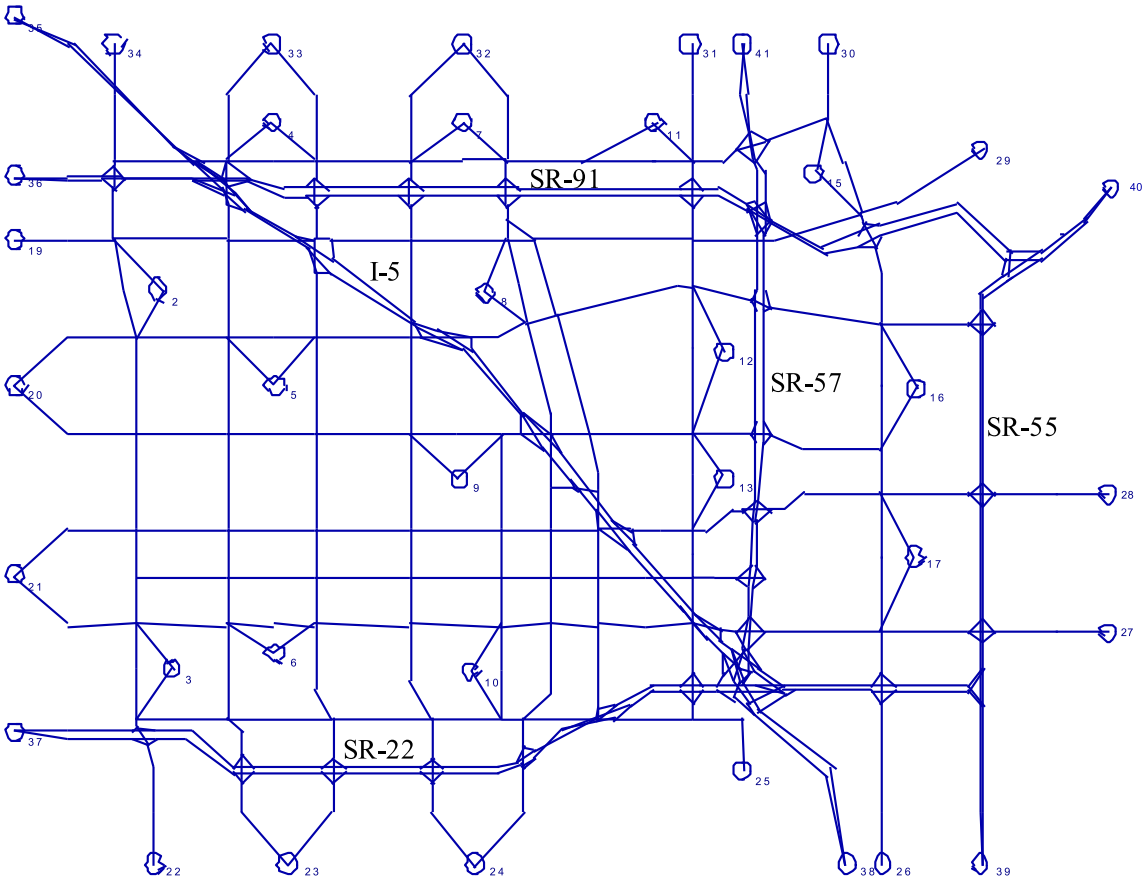

Fig. 15. The Anaheim network (Stabler, 2018).

Table 8
Social costs on the Anaheim network with various demand levels.

Scenario	1*demand	1.5*demand	2*demand	2.5*demand	3*demand
With CAV platoonable corridor	$2.9228e+8 (0.005%)				
Without CAV platoonable corridor	$2.9230e+8	$5.265e+8	$9.893e+8	$1.975e+9	$3.956e+9

1. The value displayed on the bracket represents the reduced proportion of the social cost.
2. The corridor for demand level one is (393, 394).
3. The corridor for demand level two is (181, 307).
4. The corridor for demand level three is (293, 89).
5. The corridor for demand level four is (146, 145, 144, 143, 142, 76).
6. The corridor for demand level five is (369, 353, 341, 327, 315, 299, 277, 266).

Table 9
Travel time cost and fuel costs for different vehicle classes with and without the deployed corridor.

Vehicle class	Travel time cost			Fuel cost		
	With corridor	Without corridor	Reduced proportion of travel time cost	With corridor	Without corridor	Reduced proportion of fuel cost
CAVs	$1.545e+9	$1.551e+9	0.369%	$1.958e+8	$1.960e+8	0.076%
HVs	$2.056e+9	$2.059e+9	0.167%	$1.5090e+8	$1.5089e+8	−0.010%

Because of the substantially larger network size and the increased number of O–D pairs, it takes the SACS algorithm 689,560.759 s to find the platoonable corridor, which is (633, 746, 745, 744, 743, 742, 741, 740, 712). Table 11 compares the social costs for the Winnipeg network with and without the deployed corridor. We can see that the social cost gets reduced with the deployed corridor. However, the presence of inequity cost implies that some HVs experience an increased generalized travel cost compared to that without the corridor.

Table 10
Computation time on the Anaheim network with various demand levels.

	1*demand	1.5*demand	2*demand	2.5*demand	3*demand
Computation time	328, 863.139	468, 050.192 s	638, 668.962 s	856, 474.432 s	994, 831.217 s

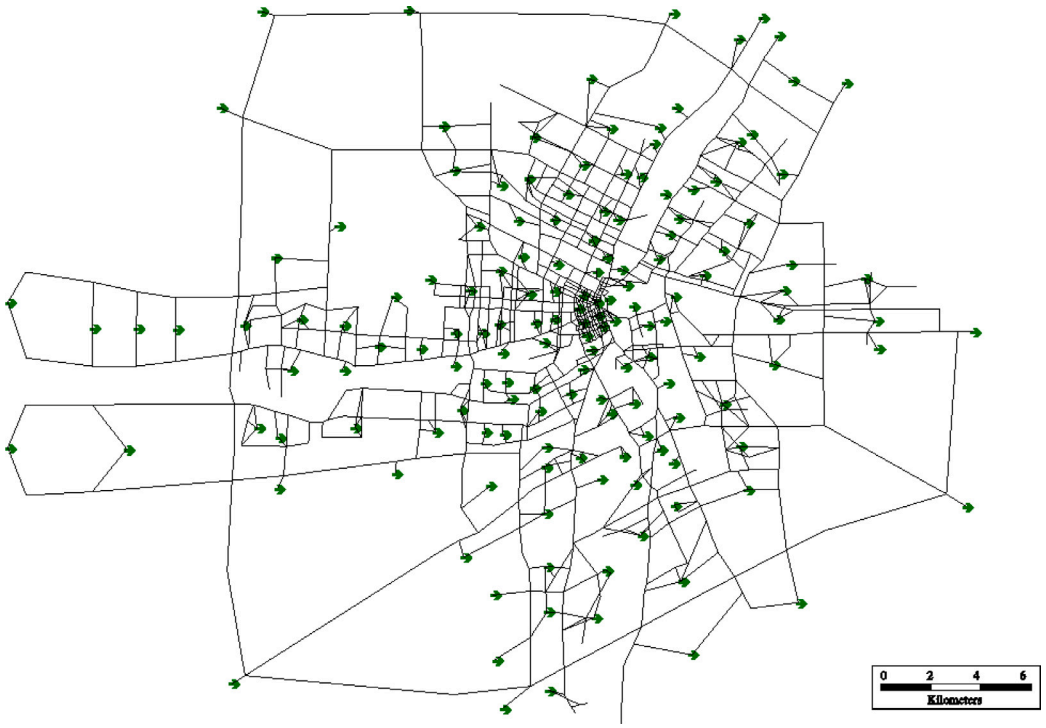

Fig. 16. The Winnipeg network (Stabler, 2018).

Table 11
Social costs with and without corridor for the Winnipeg network.

Scenario	Upgrade cost ($)	Total generalized travel cost ($)	Inequity cost ($)	Social cost ($)	The reduced cost proportion of social cost
With CAV platoonable corridor	3.732e+6	1.563e+11	3.360e+8	1.251e+11	2.202%
Without CAV platoonable corridor	0	1.599e+11	0	1.279e+11	–

4.4. A comparison of a CAV platoonable corridor and zone

Intuitively, we expect that a CAV platoonable corridor would provide a more equitable solution compared to a CAV platoonable zone (*i.e.*, a subnetwork with cycles). This is because a zone may require HVs to take longer detours, resulting in higher generalized travel costs due to the inaccessibility of the entire zone for HVs. In this section, we conduct a numerical comparison of the two designs on the ND network under a CAV market penetration ratio of 50% and a platoon size of three. To ensure a fair comparison, we let the number of CAV platoonable links be the same for both the corridor and the zone. Since the optimal corridor under this setting is $(1, 5, 9, 13, 3)$ (see the yellow area on Fig. 17), a comparable CAV platoonable zone should consist of four links. To find an optimal CAV platoonable zone with minimal social cost, we first enumerate all possible zone designs and then use the MGP algorithm to solve the corresponding equilibrium problem.

Fig. 17 depicts the optimal CAV platoonable zone and corridor on the ND network. The system cost of the zone is found to be larger than that of the corridor. To discern the cause, Table 12 compares the system performance of the two designs. The deployment of the optimal zone incurs an inequity cost, indicating that some HVs experience higher generalized travel costs. We therefore analyze which HVs are adversely affected by the CAV platoonable zone. Table 13 compares the generalized travel costs of utilized paths between each O–D pair by each vehicle class. In comparison to the scenario without the corridor, the deployed corridor leads to notable reductions in generalized travel costs for both CAVs and HVs. On the other hand, while most CAVs and HVs do benefit

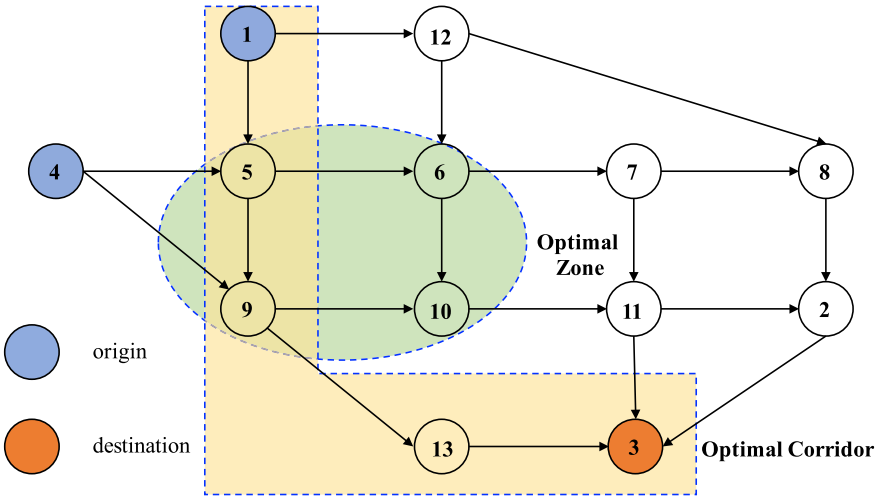

Fig. 17. The optimal CAV platoonable zone and corridor on the ND network.

Table 12
Social costs for the optimal CAV platoonable zone and corridor.

Scenario	Upgrade cost ($)	Total generalized travel cost ($)	Inequity cost ($)	Social cost ($)
With the zone	6.120e+6	2.066e+8	8.160e+6	1.704e+8
With the corridor	5.600e+6	1.663e+8	0	1.375e+8

Table 13
The generalized travel costs of utilized paths for the optimal CAV platoonable zone and corridor.

Scenario		Generalized travel cost for CAVs ($)	Generalized travel cost for HVs ($)
With the zone	(1, 3)	7.168	12.387
	(4, 3)	7.157	12.422
With the corridor	(1, 3)	5.385	10.480
	(4, 3)	5.688	9.911
Without the corridor/zone	(1, 3)	7.448	12.486
	(4, 3)	7.224	12.251

from decreased generalized travel costs when the optimal zone is introduced, the magnitude of reduction is not as prominent as that achieved with the corridor. Furthermore, the generalized travel cost for HVs with O–D pair $(4, 3)$ slightly increases with the deployment of the zone. This may be attributed to the zone providing only one viable path $(4, 9, 13, 3)$, whereas these HVs still have multiple route options available with the corridor deployed. In conclusion, the deployment of a CAV platoonable corridor yields more favorable system performance and improved equity compared to a CAV platoonable zone.

5. Conclusions

In this study, we propose the idea of an equitable CAV platoonable corridor and investigate its optimal deployment in a road network with a mixed traffic flow of CAVs and HVs. We model the problem as a Stackelberg game and formulate it as a bi-level program. At the upper level, the transportation planner leads the road users through determining the deployment of the CAV Platoonable corridor, while the road users follow by making their user-optimal route choices with the given corridor at the lower level. Considering that HV users may be worse off because road space is partially converted to dedicated infrastructure for CAVs, equity concern is incorporated in the decision-making of the CAV platoonable corridor's deployment. A platoon-embedded network equilibrium with mixed traffic (PNEMF) is developed to model travelers' route choices responding to the platoonable corridor. We further formulate the PNEMF as an equivalent VI problem and prove the existence and uniqueness of the VI solution. Finally, we propose a SACS algorithm embedded with an MGP algorithm to efficiently solve the proposed bi-level program. Our numerical results indicate that a CAV platoonable corridor can benefit all CAVs and most HVs when the CAV penetration ratio exceeds a threshold (*i.e.*, 30%).

Potential directions for future work include considering elastic additional cost and characterizing the impact of the percentage of CAVs on the road capacity under mixed traffic. From the fairness perspective, designing a subsidy policy to compensate HVs that

experience increased generalized travel costs due to the deployed corridor would be an interesting question. For a road network with a high market penetration ratio of CAVs (*e.g.,* 90%), one corridor may not be enough, so it is possible to consider deploying multiple corridors. While the SACS algorithm can be adapted to determining optimal corridors in sequence, it would be more enlightening and valuable to devise an algorithm that can concurrently determine the number and designs of necessary corridors. Additionally, future research may delve into the design of other road infrastructures, such as exclusive CAV platoonable lanes or zones, and engage in comparative studies among various designs.

Acknowledgments

The work was supported by Singapore Ministry of Education Academic Research Fund Tier 2 (MOE2019-T2-2-165), Singapore Ministry of Education Academic Research Fund Tier 1 (A-8001173-00-00) and Singapore Ministry of Education Academic Research Fund Tier 3 (MOE2019-T3-1-010). Bo Zou was also funded in part by the US National Science Foundation under grant number CMMI-2221418.

Appendix A. Proof of Proposition 1

Proof. We first prove the sufficiency part (the "if" part). This (PNEMF-VI) is clearly equivalent to

$$\begin{aligned}&\sum_{a\in A}\sum_{m\in M} g_a^m\left(v_a^*\right)v_a^m+\sum_{\tilde{w}\in\tilde{W}} g_{\tilde{w}}^{CAV}\left(\mathbf{v}^*\right)v_{\tilde{w}}^{CAV}\\ \geq&\sum_{a\in A}\sum_{m\in M} g_a^m\left(v_a^*\right)v_a^{m*}+\sum_{\tilde{w}\in\tilde{W}} g_{\tilde{w}}^{CAV}\left(\mathbf{v}^*\right)v_{\tilde{w}}^{CAV*},\quad \forall(\mathbf{h},\mathbf{x},\mathbf{v})\in\Xi.\end{aligned}$$

Thus, $(\mathbf{h}^*,\mathbf{x}^*,\mathbf{v}^*)$ are the solutions for the (PNEMF-VI) if and only if $(\mathbf{h}^*,\mathbf{x}^*,\mathbf{v}^*)$ are the solutions of the following linear optimization problem in the variables $(\mathbf{h},\mathbf{x},\mathbf{v})$ (with $(\mathbf{h}^*,\mathbf{x}^*,\mathbf{v}^*)$ considered fixed).

$$\begin{aligned}\min\quad&\sum_{a\in A}\sum_{m\in M} g_a^m\left(v_a^*\right)v_a^m+\sum_{\tilde{w}\in\tilde{W}} g_{\tilde{w}}^{CAV}\left(\mathbf{v}^*\right)v_{\tilde{w}}^{CAV}\\ s.t.\quad&(\mathbf{h},\mathbf{x},\mathbf{v})\in\Xi.\end{aligned}$$

We next write the KKT conditions of this optimization problem as followings,

$$g_a^m\left(v_a^*\right)-\zeta_a^m+\omega_a=0,\quad \forall a\in A,m\in M, \tag{30}$$

$$g_{\tilde{w}}^{CAV}\left(\mathbf{v}^*\right)-\zeta_{\tilde{w}}^{CAV}+\sum_{a\in\tilde{w}(:)}\omega_a=0,\quad \forall\tilde{w}\in\tilde{W}, \tag{31}$$

$$-\zeta_{\tilde{w}}^{HV}=0,\quad \forall\tilde{w}\in\tilde{W}, \tag{32}$$

$$-u^{w,m}+\sum_{a\in A}\xi_a^{w,m}\psi_a^r+\sum_{\tilde{w}\in\tilde{W}}\xi_{\tilde{w}}^{w,m}\psi_{\tilde{w}}^r-\rho_r^{w,m}=0,\quad \forall r\in R^{w,m},m\in M,w\in W, \tag{33}$$

$$h_r^{w,m}\rho_r^{w,m}=0,\quad \forall r\in R^{w,m},w\in W,m\in M, \tag{34}$$

$$\rho_r^{w,m}\geq 0,\quad \forall r\in R^{w,m},w\in W,m\in M, \tag{35}$$

$$-\xi_a^{w,m}+\zeta_a^m=0,\quad \forall a\in A,w\in W,m\in M, \tag{36}$$

$$-\xi_{\tilde{w}}^{w,m}+\zeta_{\tilde{w}}^m=0,\quad \forall\tilde{w}\in\tilde{W},w\in W,m\in M, \tag{37}$$

$$-\omega_a=0,\quad \forall a\in A^0, \tag{38}$$

$$(\mathbf{h},\mathbf{x},\mathbf{v})\in\Xi,$$

where $u^{w,m}$, $\rho_r^{w,m}$, $\xi_a^{w,m}$, $\xi_{\tilde{w}}^{w,m}$, ζ_a^m, and $\zeta_{\tilde{w}}^m$ are the Lagrange multipliers for constraints (11), (12), (13), (14), (15) and (16), respectively. ω_a is the Lagrange multiplier for constraints (17) and (18), From (30), (36), (38), we have

$$g_a^m\left(v_a^*\right)=\xi_a^{w,m},\quad \forall a\in A,w\in W,m\in M. \tag{39}$$

From (31), (37), and (38), we have

$$g_{\tilde{w}}^{CAV}\left(\mathbf{v}^*\right)=\xi_{\tilde{w}}^{w,CAV},\quad \forall\tilde{w}\in\tilde{W},w\in W. \tag{40}$$

From (32) and (37), we have

$$\xi_{\tilde{w}}^{w,HV}=0,\quad \forall\tilde{w}\in\tilde{W},w\in W. \tag{41}$$

From (33), (34), (39) and (40), we have

$$\left(\sum_{a\in A} g_a^{CAV}\left(v_a^*\right)\psi_a^r+\sum_{\tilde{w}\in\tilde{W}} g_{\tilde{w}}^{CAV}\left(\mathbf{v}^*\right)\psi_{\tilde{w}}^r-u^{w,CAV}\right)h_r^{w,CAV}=0,\quad \forall r\in R^{w,CAV},w\in W. \tag{42}$$

From (33), (35), (39) and (40), we have

$$\sum_{a\in A} g_a^{CAV}\left(v_a^*\right)\psi_a^r + \sum_{\tilde{w}\in\tilde{W}} g_{\tilde{w}}^{CAV}\left(\mathbf{v}^*\right)\psi_{\tilde{w}}^r - u^{w,CAV} \geq 0, \quad \forall r \in R^{w,CAV}, w \in W. \tag{43}$$

From (33), (34), (39) and (41), we have

$$\left(\sum_{a\in A} g_a^{HV}\left(v_a^*\right)\psi_a^r - u^{w,HV}\right) h_r^{w,HV} = 0, \quad \forall r \in R^{w,HV}, w \in W. \tag{44}$$

From (33), (35), (39) and (41), we have

$$\sum_{a\in A} g_a^{HV}\left(v_a^*\right)\psi_a^r - u^{w,HV} \geq 0, \quad \forall r \in R^{w,HV}, w \in W. \tag{45}$$

By noting that (42)–(45) are complementary slackness conditions correspond to (7)–(10), the first half of the proof is completed.

We next prove the necessary part (the "only if" part). Suppose that the solution $(\mathbf{h}^*, \mathbf{x}^*, \mathbf{v}^*) \in \Xi$ satisfies conditions (7)–(10), then we have

$$\left(\sum_{a\in A} g_a^{w,CAV}(v_a^*)\psi_a^r + \sum_{\tilde{w}\in\tilde{W}} g_{\tilde{w}}^{w,CAV}(\mathbf{v}^*)\psi_{\tilde{w}}^r - u^{w,CAV}\right) h_r^{w,CAV*} = 0, \ \forall r \in R^{w,CAV}, w \in W, \tag{46}$$

$$\left(\sum_{a\in A} g_a^{w,HV}(v_a*)\psi_a^r - u^{w,HV}\right) h_r^{w,HV*} = 0, \ \forall r \in R^{w,HV}, w \in W, \tag{47}$$

$$\sum_{a\in A} g_a^{w,CAV}(v_a^*)\psi_a^r + \sum_{\tilde{w}\in\tilde{W}} g_{\tilde{w}}^{w,CAV}(\mathbf{v}^*)\psi_{\tilde{w}}^r - u^{w,CAV} \geq 0, \ \forall r \in R^{w,CAV}, w \in W, \tag{48}$$

$$\sum_{a\in A} g_a^{w,HV}(v_a^*)\psi_a^r - u^{w,HV} \geq 0, \forall r \in R^{w,HV}, w \in W. \tag{49}$$

For any feasible solution $(\mathbf{h}, \mathbf{x}, \mathbf{v}) \in \Xi$, we can derive the followings based on (48)–(49),

$$\left(\sum_{a\in A} g_a^{w,CAV}(v_a^*)\psi_a^r + \sum_{\tilde{w}\in\tilde{W}} g_{\tilde{w}}^{w,CAV}(\mathbf{v}^*)\psi_{\tilde{w}}^r - u^{w,CAV}\right) h_r^{w,CAV} \geq 0, \ \forall r \in R^{w,CAV}, w \in W, \tag{50}$$

$$\left(\sum_{a\in A} g_a^{w,HV}(v_a*)\psi_a^r - u^{w,HV}\right) h_r^{w,HV} \geq 0, \ \forall r \in R^{w,HV}, w \in W. \tag{51}$$

Using (46)–(47) and (50)–(51), we have

$$\left(\sum_{a\in A} g_a^{CAV}(v_a^*)\psi_a^r + \sum_{\tilde{w}\in\tilde{W}} g_{\tilde{w}}^{CAV}(\mathbf{v}^*)\psi_{\tilde{w}}^r - u^{w,CAV}\right)\left(h_r^{w,CAV} - h_r^{w,CAV*}\right) \geq 0, \quad \forall r \in R^{w,CAV}, w \in W, \tag{52}$$

$$\left(\sum_{a\in A} g_a^{HV}(v_a^*)\psi_a^r - u^{w,HV}\right)\left(h_r^{w,HV} - h_r^{w,HV*}\right) \geq 0, \quad \forall r \in R^{w,HV}, w \in W. \tag{53}$$

For all $(\mathbf{h}, \mathbf{x}, \mathbf{v}) \in \Xi$, summing up the inequalities (52) and (53) over all feasible paths, O–D pairs

$$\begin{aligned}&\sum_{w\in W}\sum_{r\in R^{w,CAV}}\left(\sum_{a\in A} g_a^{CAV}(v_a^*)\psi_a^r + \sum_{\tilde{w}\in\tilde{W}} g_{\tilde{w}}^{CAV}(\mathbf{v}^*)\psi_{\tilde{w}}^r - u^{w,CAV}\right)\left(h_r^{w,CAV} - h_r^{w,CAV*}\right)\\ &+ \sum_{w\in W}\sum_{r\in R^{w,HV}}\left(\sum_{a\in A} g_a^{HV}(v_a^*)\psi_a^r - u^{w,HV}\right)\left(h_r^{w,HV} - h_r^{w,HV*}\right) \geq 0.\end{aligned} \tag{54}$$

For each vehicle class $m \in M$, the following equation holds for each O–D pair $w \in W$,

$$\sum_{r\in R^{w,m}}\left(h_r^{w,m} - h_r^{w,m*}\right) = 0. \tag{55}$$

This is because for any O–D pair $w \in W$ by any vehicle class $m \in M$, the values of $\sum_{r\in R^{w,m}} h_r^{w,m}$ for all $\mathbf{h}$ that satisfies (11) are identical and equal to $q^{w,m}$. Based on (55), the inequality (54) can be simplified as

$$\begin{aligned}&\sum_{w\in W}\sum_{r\in R^{w,CAV}}\left(\sum_{a\in A} g_a^{CAV}(v_a^*)\psi_a^r + \sum_{\tilde{w}\in\tilde{W}} g_{\tilde{w}}^{CAV}(\mathbf{v}^*)\psi_{\tilde{w}}^r\right)\left(h_r^{w,CAV} - h_r^{w,CAV*}\right)\\ &+ \sum_{w\in W}\sum_{r\in R^{w,HV}}\left(\sum_{a\in A} g_a^{HV}(v_a^*)\psi_a^r\right)\left(h_r^{w,HV} - h_r^{w,HV*}\right) \geq 0.\end{aligned} \tag{56}$$

Using (13)–(16), the above inequality can be expressed in terms of the aggregate flows, *i.e.*,

$$\sum_{a\in A}\sum_{m\in M} g_a^m\left(v_a^*\right)\left(v_a^m - v_a^{m*}\right) + \sum_{\tilde{w}\in\tilde{W}} g_{\tilde{w}}^{CAV}\left(\mathbf{v}^*\right)\left(v_{\tilde{w}}^{CAV} - v_{\tilde{w}}^{CAV*}\right) \geq 0.$$

This is exactly (PNEMF-VI), which completes the proof. □

Appendix B. Proof of Proposition 2

Proof. By construction, the feasible set Ξ is a bounded polyhedron (*i.e.*, a polytope) because the demands $q^{w,m}$ for all $w \in w, m \in M$ are finite. Moreover, Ξ is non-empty because it is assumed that all vehicles can reach their respective destinations. Since the link travel time function is continuous, the generalized travel costs on link $a \in A$ and E–E pair $\tilde{w} \in \tilde{W}$ are also continuous. Therefore, (PNEMF-VI) admits at least one solution by invoking Theorem 1.4 in Nagurney (1998). □

Appendix C. Proof of Proposition 3

Proof. We first divide (1) by λ_m, and divide (2) by λ_{CAV} to obtain the followings:

$$\begin{cases} \tilde{g}_a^m(v_a) = t_a(v_a) + \frac{1}{\lambda_m} f_a^m, & \forall m \in M, a \in A, \quad \text{(a)} \\ \tilde{g}_{\tilde{w}}^{CAV}(\mathbf{v}) = \sum_{a \in \tilde{w}(:)} \left(t_a\left(v_a\right) + \frac{1}{\lambda_{CAV}} f_a^{CAV} \right) + \frac{1}{\lambda_{CAV}} \tau_{\tilde{w}}, & \forall \tilde{w} \in \tilde{W}, \quad \text{(b)} \end{cases} \tag{57}$$

where we denote $\tilde{g}_a^m(v_a)$ and $\tilde{g}_{\tilde{w}}^{CAV}(\mathbf{v})$ as the generalized travel time on the non-platoonable link $a \in A$ for class $m \in M$ and the E–E pair $\tilde{w} \in \tilde{W}$, respectively. Then, the time-based UE conditions for any feasible solution $(\mathbf{h}, \mathbf{x}, \mathbf{v}) \in \Xi$ are:

$$\sum_{a \in A} \tilde{g}_a^{CAV}(v_a)\psi_a^r + \sum_{\tilde{w} \in \tilde{W}} \tilde{g}_{\tilde{w}}^{CAV}(\mathbf{v})\psi_{\tilde{w}}^r = \tilde{u}^{w,CAV}, \quad \text{if } h_r^{w,CAV} > 0, r \in R^{w,CAV}, w \in W, \tag{58}$$

$$\sum_{a \in A} \tilde{g}_a^{CAV}(v_a)\psi_a^r + \sum_{\tilde{w} \in \tilde{W}} \tilde{g}_{\tilde{w}}^{CAV}(\mathbf{v})\psi_{\tilde{w}}^r \geq \tilde{u}^{w,CAV}, \quad \text{if } h_r^{w,CAV} = 0, r \in R^{w,CAV}, w \in W, \tag{59}$$

$$\sum_{a \in A} \tilde{g}_a^{HV}(v_a)\psi_a^r = \tilde{u}^{w,HV} \quad \text{if } h_r^{w,HV} > 0, r \in R^{w,HV}, w \in W, \tag{60}$$

$$\sum_{a \in A} \tilde{g}_a^{HV}(v_a)\psi_a^r > \tilde{u}^{w,HV}, \quad \text{if } h_r^{w,HV} = 0, r \in R^{w,HV}, w \in W, \tag{61}$$

where $\tilde{u}^{w,m}$ is the minimum generalized travel time for the time-based UE. Analogous to the proof of Proposition 1, the equivalent time-based VI problem is

$$\sum_{a \in A} \sum_{m \in M} \tilde{g}_a^m(v_a^*)\left(v_a^m - v_a^{m*}\right) + \sum_{\tilde{w} \in \tilde{W}} \tilde{g}_{\tilde{w}}^{CAV}(\mathbf{v}^*)(v_{\tilde{w}}^{CAV} - v_{\tilde{w}}^{CAV*}) \geq 0, \quad \forall (\mathbf{h}, \mathbf{x}, \mathbf{v}) \in \Xi. \tag{62}$$

Suppose that $(\mathbf{h}^{**}, \mathbf{x}^{**}, \mathbf{v}^{**})$ is also a solution of (62), and $(\mathbf{h}^*, \mathbf{x}^*, \mathbf{v}^*) \neq (\mathbf{h}^{**}, \mathbf{x}^{**}, \mathbf{v}^{**})$, then we have

$$\sum_{a \in A} \sum_{m \in M} \tilde{g}_a^m(v_a^{**})\left(v_a^m - v_a^{m**}\right) + \sum_{\tilde{w} \in \tilde{W}} \tilde{g}_{\tilde{w}}^{CAV}(\mathbf{v}^{**})(v_{\tilde{w}}^{CAV} - v_{\tilde{w}}^{CAV**}) \geq 0, \quad \forall (\mathbf{h}, \mathbf{x}, \mathbf{v}) \in \Xi. \tag{63}$$

Let $(\mathbf{h}, \mathbf{x}, \mathbf{v})$ in (62) be $(\mathbf{h}^{**}, \mathbf{x}^{**}, \mathbf{v}^{**})$ and $(\mathbf{h}, \mathbf{x}, \mathbf{v})$ in (63) be $(\mathbf{h}^*, \mathbf{x}^*, \mathbf{v}^*)$, then we have

$$\sum_{a \in A} \sum_{m \in M} \tilde{g}_a^m(v_a^*)\left(v_a^{m**} - v_a^{m*}\right) + \sum_{\tilde{w} \in \tilde{W}} \tilde{g}_{\tilde{w}}^{CAV}(\mathbf{v}^*)(v_{\tilde{w}}^{CAV**} - v_{\tilde{w}}^{CAV*}) \geq 0, \tag{64}$$

$$\sum_{a \in A} \sum_{m \in M} \tilde{g}_a^m(v_a^{**})\left(v_a^{m*} - v_a^{m**}\right) + \sum_{\tilde{w} \in \tilde{W}} \tilde{g}_{\tilde{w}}^{CAV}(\mathbf{v}^{**})(v_{\tilde{w}}^{CAV*} - v_{\tilde{w}}^{CAV**}) \geq 0. \tag{65}$$

Using (57)(a)–(57)(b), we reformulate (64) and (65), and have

$$\begin{aligned} &- \sum_{a \in A} \left(\left(t_a(v_a^*) + \frac{1}{\lambda_{HV}} f_a^{HV} \right) \left(v_a^{HV**} - v_a^{HV*} \right) + \left(t_a(v_a^*) + \frac{1}{\lambda_{CAV}} f_a^{CAV} \right) \left(v_a^{CAV**} - v_a^{CAV*} \right) \right) \\ &- \sum_{\tilde{w} \in \tilde{W}} \left(\sum_{a \in \tilde{A}: a \in \tilde{w}(:)} \left(t_a\left(v_a^*\right) + \frac{1}{\lambda_{CAV}} f_a^{CAV} \right) + \tau_{\tilde{w}} \frac{1}{\lambda_{CAV}} \right) \left(v_{\tilde{w}}^{CAV**} - v_{\tilde{w}}^{CAV*} \right) \leq 0, \\ &\sum_{a \in A} \left(\left(t_a(v_a^{**}) + \frac{1}{\lambda_{HV}} f_a^{HV} \right) \left(v_a^{HV**} - v_a^{HV*} \right) + \left(t_a(v_a^{**}) + \frac{1}{\lambda_{CAV}} f_a^{CAV} \right) \left(v_a^{CAV**} - v_a^{CAV*} \right) \right) \\ &+ \sum_{\tilde{w} \in \tilde{W}} \left(\sum_{a \in \tilde{A}: a \in \tilde{w}(:)} \left(t_a\left(v_a^{**}\right) + \frac{1}{\lambda_{CAV}} f_a^{CAV} \right) + \tau_{\tilde{w}} \frac{1}{\lambda_{CAV}} \right) \left(v_{\tilde{w}}^{CAV**} - v_{\tilde{w}}^{CAV*} \right) \leq 0. \end{aligned}$$

Because of (17)–(18), the above two inequalities can be expressed based on aggregate link flow v_a on link $a \in A \cup \tilde{A}$:

$$\sum_{a \in A^0} \left(t_a(v_a^{**}) - t_a(v_a^*) \right) \left(v_a^{**} - v_a^* \right) \leq 0,$$

which contradicts our assumption that the travel time function is strictly increasing. Hence, we have $\left(v_a^{**}\right)_{a \in A^0} = \left(v_a^*\right)_{a \in A^0}$, and we can claim that the aggregate link flow is unique for the time-based VI problem. That being said, $(v_a)_{a \in A^0}$ is unique for the time-based platoon-embedded equilibrium (*i.e.*, (11)–(18), (58)–(61)). By invoking Theorem 2.3 in Yang and Huang (2005), the

solutions satisfying time-based constraints ((11)–(18) and (58)–(61)) and monetary-based equilibrium constraints ((7)–(18)) are identical in any general network if and only if users of each class have a constant VoT (VoTs for different user classes can be different). Therefore, the aggregate link flow is unique for the monetary-based equilibrium. This completes the proof. □

Appendix D. KKT conditions for the optimization problem

$$t_a(v_a) - \zeta_a = 0, \quad \forall a \in A, \tag{66}$$

$$t_a(v_a) - \zeta_a + f_a^{CAV}\frac{1}{\lambda_{CAV}} = 0, \quad \forall a \in \tilde{A}, \tag{67}$$

$$f_a^m \frac{1}{\lambda_m} - \zeta_a^m + \zeta_a = 0, \quad \forall a \in A, m \in M, \tag{68}$$

$$\frac{1}{\lambda_{CAV}}\tau_{\tilde{w}} - \zeta_{\tilde{w}}^{CAV} + \sum_{a\in\tilde{w}(:)} \zeta_a = 0, \quad \forall \tilde{w} \in \tilde{W}, \tag{69}$$

$$-\xi_a^{w,m} + \zeta_a^m = 0, \quad \forall a \in A, w \in W, m \in M, \tag{70}$$

$$-\xi_{\tilde{w}}^{w,CAV} + \zeta_{\tilde{w}}^{CAV} = 0, \quad \forall \tilde{w} \in \tilde{W}, w \in W, \tag{71}$$

$$\rho_r^{w,m} \geq 0, \quad \forall r \in R^{w,m}, w \in W, m \in M, \tag{72}$$

$$\rho_r^{w,m} h_r^{w,m} = 0, \quad \forall r \in R^{w,m}, w \in W, m \in M, \tag{73}$$

$$-\hat{u}^{w,HV} - \rho_r^{w,HV} + \sum_{a\in A} \xi_a^{w,HV}\psi_a^r = 0, \quad \forall r \in R^{w,HV}, w \in W, \tag{74}$$

$$-\hat{u}^{w,CAV} - \rho_r^{w,CAV} + \sum_{a\in A} \xi_a^{w,CAV}\psi_a^r + \sum_{\tilde{w}\in\tilde{W}} \xi_{\tilde{w}}^{w,CAV}\psi_{\tilde{w}}^r = 0, \quad \forall r \in R^{w,CAV}, w \in W, \tag{75}$$

(11)–(18),

where $\hat{u}^{w,m}$, $\rho_r^{w,m}$, $\xi_a^{w,m}$, $\xi_{\tilde{w}}^{w,CAV}$, ζ_a^m, and $\zeta_{\tilde{w}}^{CAV}$ are the Lagrange multipliers for constraints (11), (12), (13), (14), (15) and (16), respectively. ζ_a is the Lagrange multiplier for constraints (17) and (18). From (66), (68), (70), we have

$$\xi_a^{w,m} = t_a(v_a) + f_a^m \frac{1}{\lambda_m}, \quad \forall a \in A, w \in W, m \in M. \tag{76}$$

From (67), (69), (71), we have

$$\xi_{\tilde{w}}^{w,CAV} = \sum_{a\in\tilde{w}(:)} \left(t_a(v_a) + f_a^{CAV}\frac{1}{\lambda_{CAV}}\right) + \frac{1}{\lambda_{CAV}}\tau_{\tilde{w}}, \quad \forall \tilde{w} \in \tilde{W}, w \in W. \tag{77}$$

Then from (72), (74), and (76), we have

$$\sum_{a\in A}\left(t_a(v_a) + f_a^{HV}\frac{1}{\lambda_{HV}}\right)\psi_a^r - \hat{u}^{w,HV} \geq 0. \quad \forall r \in R^{w,HV}, w \in W. \tag{78}$$

From (73), (74), and (76), we have

$$\left(\sum_{a\in A}\left(t_a(v_a) + f_a^{HV}\frac{1}{\lambda_{HV}}\right)\psi_a^r - \hat{u}^{w,HV}\right)h_r^{w,HV} = 0. \quad \forall r \in R^{w,HV}, w \in W. \tag{79}$$

From (72), (75) and (76)–(77), we have

$$\sum_{a\in A}\left(t_a(v_a) + f_a^{CAV}\frac{1}{\lambda_{CAV}}\right)\psi_a^r + \sum_{\tilde{w}\in\tilde{W}}\left(\sum_{a\in\tilde{w}(:)}\left(t_a(v_a) + f_a^{CAV}\frac{1}{\lambda_{CAV}}\right) + \frac{1}{\lambda_{CAV}}\tau_{\tilde{w}}\right)\psi_{\tilde{w}}^r - \hat{u}^{w,CAV} \geq 0,$$
$$\forall r \in R^{w,CAV}, w \in W. \tag{80}$$

From (73), (75) and (76)–(77), we have

$$\left(\sum_{a\in A}\left(t_a(v_a) + f_a^{CAV}\frac{1}{\lambda_{CAV}}\right)\psi_a^r + \sum_{\tilde{w}\in\tilde{W}}\left(\sum_{a\in\tilde{w}(:)}\left(t_a(v_a) + f_a^{CAV}\frac{1}{\lambda_{CAV}}\right) + \frac{1}{\lambda_{CAV}}\tau_{\tilde{w}}\right)\psi_{\tilde{w}}^r - \hat{u}^{w,CAV}\right)h_r^{w,CAV}$$
$$=0, \quad \forall r \in R^{w,CAV}, w \in W. \tag{81}$$

Then we multiply (78)–(79) with λ_{HV}, and multiply (80)–(81) with λ_{CAV}. Since $g_a^m(v_a) = t_a(v_a)\lambda_m + f_a^m, \forall a \in A, m \in M$, and $g_{\tilde{w}}^{CAV}(\mathbf{v}) = \left(\sum_{a\in\tilde{w}(:)}\left(t_a(v_a)\lambda_{CAV} + f_a^{CAV}\right) + \tau_{\tilde{w}}\right), \forall \tilde{w} \in \tilde{W}$, we have

$$\sum_{a\in A} g_a^{w,HV}(v_a)\psi_a^r - u^{w,HV}\lambda_{HV} \geq 0, \quad \forall r \in R^{w,HV}, w \in W, \tag{82}$$

Table 14
Link characteristics of the ND network.

Link	l_a(miles)	t_a^0(min)	Link	l_a(miles)	t_a^0(min)	Link	l_a(miles)	t_a^0(min)
(1, 5)	5.8	7	(6, 7)	8	6	(10, 11)	6	6
(1, 12)	7.5	9	(6, 10)	10.8	13	(11, 2)	5.8	7
(2, 3)	10	12	(7, 8)	8.3	10	(11, 3)	6.7	8
(4, 5)	7.5	9	(7, 11)	7.5	9	(12, 6)	5.8	7
(4, 9)	10	12	(8, 2)	7.5	9	(12, 8)	11.7	14
(5, 6)	6	8	(9, 10)	8.3	10	(13, 3)	9.2	11
(5, 9)	5.5	9	(9, 13)	7.5	9			

Table 15
Fuel saving of platooning vehicles.

Platoon size(s)	Vehicle position in a platoon*	The proportion of fuel saving δ^*
2	1	0%
	2	6%
	Average	3%
3, 4*, 5*	1	0%
	2	5%
	3, 4, 5	8%
	Average(3-AV platoon)	4.4%
	Average(4-AV platoon)	5.3%
	Average(5-AV platoon)	5.8%

1. 1 refers to the leading CAV, 2 refers to the CAV right behind the leading CAV, etc.
2. δ values for four, five CAV platooning cases are derived by assuming that the trailing CAVs in positions 3, 4, 5 have the same fuel savings (Hussein and Rakha, 2021).
3. For larger platoon sizes (*i.e.*, 6, 7, 8, 9, 10, 11, 12, 13, 14, 15), we roughly assume the trailing CAVs in positions 6, 7, 8, 9, 10, 11, 12, 13, 14, 15 have the same fuel savings.

$$\left(\sum_{a\in A} g_a^{w,HV}(v_a)\psi_a^r - u^{w,HV}\lambda_{HV}\right) h_r^{w,HV} = 0, \quad \forall r \in R^{w,HV}, w \in W, \tag{83}$$

$$\sum_{a\in A} g_a^{w,CAV}(v_a)\psi_a^r + \sum_{\tilde{w}\in\tilde{W}} g_{\tilde{w}}^{w,CAV}(\mathbf{v})\psi_{\tilde{w}}^r - u^{w,CAV}\lambda_{CAV} \geq 0, \quad \forall r \in R^{w,CAV}, w \in W, \tag{84}$$

$$\left(\sum_{a\in A} g_a^{w,CAV}(v_a)\psi_a^r + \sum_{\tilde{w}\in\tilde{W}} g_{\tilde{w}}^{w,CAV}(\mathbf{v})\psi_{\tilde{w}}^r - u^{w,CAV}\lambda_{CAV}\right) h_r^{w,CAV} = 0, \quad \forall r \in R^{w,CAV}, w \in W, \tag{85}$$

where $u^{w,m}$ is derived by scaling $\hat{u}^{w,m}$ by λ_m. From (82) and (84), we can see that $u^{w,m}$ is less than or equal to the generalized travel cost between O–D pair $w \in W$ by vehicle class $m \in M$. From (83) and (85), it represents the generalized travel cost for utilized paths based on the assumption that $R^{w,m} \neq \emptyset$ and $q^{w,m} > 0$. Thus, it is the minimum generalized travel cost for the utilized paths. Note that (82)–(85) are identically (7)–(10). This completes the proof.

Appendix E. Numerical parameter settings

See Tables 14 and 15.

References

Abdolmaleki, Mojtaba, Shahabi, Mehrdad, Yin, Yafeng, Masoud, Neda, 2019. Itinerary planning for cooperative truck platooning. 3481598, Available at SSRN.

Babazadeh, Abbas, Poorzahedy, Hossain, Nikoosokhan, Saeid, 2011. Application of particle swarm optimization to transportation network design problem. J. King Saud Univ.-Sci. 23 (3), 293–300.

Van den Berg, Vincent A.C., Verhoef, Erik T., 2016. Autonomous cars and dynamic bottleneck congestion: The effects on capacity, value of time and preference heterogeneity. Transp. Res. B 94, 43–60.

Berry, Irene Michelle, 2010. The effects of driving style and vehicle performance on the real-world fuel consumption of US light-duty vehicles (Ph.D. thesis). Massachusetts Institute of Technology.

Bibeka, Apoorba, Songchitruksa, Praprut, Zhang, Yunlong, 2021. Assessing environmental impacts of ad-hoc truck platooning on multilane freeways. J. Intell. Transp. Syst. 25 (3), 281–292.

Černỳ, Vladimír, 1985. Thermodynamical approach to the traveling salesman problem: An efficient simulation algorithm. J. Optim. Theory Appl. 45 (1), 41–51.

Chang, Ben-Jye, Chiou, Jhih-Ming, 2019. Cloud computing-based analyses to predict vehicle driving shockwave for active safe driving in intelligent transportation system. IEEE Trans. Intell. Transp. Syst. 21 (2), 852–866.

Chen, Danjue, Ahn, Soyoung, Chitturi, Madhav, Noyce, David A., 2017a. Towards vehicle automation: Roadway capacity formulation for traffic mixed with regular and automated vehicles. Transp. Res. B 100, 196–221.

Chen, Zhibin, He, Fang, Yin, Yafeng, Du, Yuchuan, 2017b. Optimal design of autonomous vehicle zones in transportation networks. Transp. Res. B 99, 44–61.

Chen, Zhibin, He, Fang, Zhang, Lihui, Yin, Yafeng, 2016. Optimal deployment of autonomous vehicle lanes with endogenous market penetration. Transp. Res. C 72, 143–156.

Chen, Anthony, Lee, Der-Horng, Jayakrishnan, R., 2002. Computational study of state-of-the-art path-based traffic assignment algorithms. Math. Comput. Simul. 59 (6), 509–518.
Chen, Anthony, Zhou, Zhong, Xu, Xiangdong, 2012. A self-adaptive gradient projection algorithm for the nonadditive traffic equilibrium problem. Comput. Oper. Res. 39 (2), 127–138.
Cunha, Maria da Conceição, Sousa, Joaquim, 1999. Water distribution network design optimization: simulated annealing approach. J. Water Resour. Plan. Manag. 125 (4), 215–221.
Darbha, Swaroop, Konduri, Shyamprasad, Pagilla, Prabhakar R., 2018. Benefits of V2V communication for autonomous and connected vehicles. IEEE Trans. Intell. Transp. Syst. 20 (5), 1954–1963.
Delahaye, Daniel, Chaimatanan, Supatcha, Mongeau, Marcel, 2019. Simulated annealing: From basics to applications. Handb. Metaheuristics 1–35.
Do, Wooseok, Rouhani, Omid M., Miranda-Moreno, Luis, 2019. Simulation-based connected and automated vehicle models on highway sections: a literature review. J. Adv. Transp. 2019.
Farah, Haneen, Koutsopoulos, Haris N., 2014. Do cooperative systems make drivers' car-following behavior safer? Transp. Res. C 41, 61–72.
Feng, Yijia, He, Dazhi, Guan, Yunfeng, 2019. Composite platoon trajectory planning strategy for intersection throughput maximization. IEEE Trans. Veh. Technol. 68 (7), 6305–6319.
Gao, Ziyou, Wu, Jianjun, Sun, Huijun, 2005. Solution algorithm for the bi-level discrete network design problem. Transp. Res. B 39 (6), 479–495.
Gentile, Guido, 2014. Local user cost equilibrium: a bush-based algorithm for traffic assignment. Transp. A: Transp. Sci. 10 (1), 15–54.
Ghamami, Mehrnaz, Zockaie, Ali, Nie, Yu Marco, 2016. A general corridor model for designing plug-in electric vehicle charging infrastructure to support intercity travel. Transp. Res. C 68, 389–402.
Gong, Siyuan, Shen, Jinglai, Du, Lili, 2016. Constrained optimization and distributed computation based car following control of a connected and autonomous vehicle platoon. Transp. Res. B 94, 314–334.
Hall, Randolph, Chin, Chinan, 2005. Vehicle sorting for platoon formation: Impacts on highway entry and throughput. Transp. Res. C 13 (5), 405–420.
He, Anqi, Wang, Lifeng, Chen, Yue, Wong, Kai-Kit, Elkashlan, Maged, 2017. Spectral and energy efficiency of uplink D2D underlaid massive MIMO cellular networks. IEEE Trans. Commun. 65 (9), 3780–3793.
Hu, Xiaoyan, Wang, Lifeng, Wong, Kai-Kit, Tao, Meixia, Zhang, Yangyang, Zheng, Zhongbin, 2019. Edge and central cloud computing: A perfect pairing for high energy efficiency and low-latency. IEEE Trans. Wireless Commun. 19 (2), 1070–1083.
Hussein, Ahmed, Rakha, Hesham, 2021. Vehicle platooning impact on drag coefficients and energy/fuel saving implications. IEEE Trans. Veh. Technol..
Jayakrishnan, R., Tsai, Wei T., Prashker, Joseph N., Rajadhyaksha, Subodh, 1994. A faster path-based algorithm for traffic assignment. Transp. Res. Board 1443, 75–83.
Johansson, Alexander, Mårtensson, Jonas, Sun, Xiaotong, Yin, Yafeng, 2021a. Real-time cross-fleet Pareto-improving truck platoon coordination. In: 2021 IEEE International Intelligent Transportation Systems Conference (ITSC). IEEE, pp. 996–1003.
Johansson, Alexander, Nekouei, Ehsan, Johansson, Karl Henrik, Mårtensson, Jonas, 2018. Multi-fleet platoon matching: A game-theoretic approach. In: 2018 21st International Conference on Intelligent Transportation Systems (ITSC). IEEE, pp. 2980–2985.
Johansson, Alexander, Nekouei, Ehsan, Johansson, Karl Henrik, Mårtensson, Jonas, 2021b. Strategic hub-based platoon coordination under uncertain travel times. IEEE Trans. Intell. Transp. Syst..
Khattak, Asad J., Wali, Behram, 2017. Analysis of volatility in driving regimes extracted from basic safety messages transmitted between connected vehicles. Transp. Res. C 84, 48–73.
Khoder, Rami, Naja, Rola, Tohme, Samir, 2020. Performance evaluation of speed platoon splitting algorithm. In: Vehicular Ad-Hoc Networks for Smart Cities. Springer, pp. 31–42.
Kim, Yong Hoon, Peeta, Srinivas, He, Xiaozheng, 2017. Modeling the information flow propagation wave under vehicle-to-vehicle communications. Transp. Res. C 85, 377–395.
Kirkpatrick, Scott, Gelatt, C. Daniel, Vecchi, Mario P., 1983. Optimization by simulated annealing. science 220 (4598), 671–680.
Kumbharana, N., Pandey, Gopal M., 2013. A comparative study of ACO, GA and SA for solving travelling salesman problem. Int. J. Soc. Appl. Comput. Sci. 2 (2), 224–228.
Larsen, Rune, Rich, Jeppe, Rasmussen, Thomas Kjær, 2019. Hub-based truck platooning: Potentials and profitability. Transp. Res. E 127, 249–264.
Laval, Jorge A., Leclercq, Ludovic, 2010. A mechanism to describe the formation and propagation of stop-and-go waves in congested freeway traffic. Phil. Trans. R. Soc. A 368 (1928), 4519–4541.
Leblanc, Larry J., 1975. An algorithm for the discrete network design problem. Transp. Sci. 9 (3), 183–199.
Lee, Yi-Ching, Momen, Ali, LaFreniere, Jennifer, 2021. Attributions of social interactions: Driving among self-driving vs. conventional vehicles. Technol. Soc. 66, 101631.
Li, Ye, Chen, Zhibin, Yin, Yafeng, Peeta, Srinivas, 2020. Deployment of roadside units to overcome connectivity gap in transportation networks with mixed traffic. Transp. Res. C 111, 496–512.
Liang, Kuo-Yun, Mårtensson, Jonas, Johansson, Karl H., 2015. Heavy-duty vehicle platoon formation for fuel efficiency. IEEE Trans. Intell. Transp. Syst. 17 (4), 1051–1061.
Lin, Yu-Yu, Rubin, Izhak, 2017. Infrastructure aided networking and traffic management for autonomous transportation. In: 2017 Information Theory and Applications Workshop (ITA). IEEE, pp. 1–7.
Litman, Todd, 2020. Autonomous vehicle implementation predictions: Implications for transport planning. Transp. Res. Board.
Liu, Zhaocai, Chen, Zhibin, He, Yi, Song, Ziqi, 2021. Network user equilibrium problems with infrastructure-enabled autonomy. Transp. Res. B 154, 207–241.
Liu, Hao, Kan, Xingan, Shladover, Steven E., Lu, Xiao-Yun, Ferlis, Robert E., 2018. Impact of cooperative adaptive cruise control on multilane freeway merge capacity. J. Intell. Transp. Syst. 22 (3), 263–275.
Liu, Zhaocai, Song, Ziqi, 2019. Strategic planning of dedicated autonomous vehicle lanes and autonomous vehicle/toll lanes in transportation networks. Transp. Res. C 106, 381–403.
Liu, Meiqi, Wang, Meng, Hoogendoorn, Serge, 2019. Optimal platoon trajectory planning approach at arterials. Transp. Res. Rec. 2673 (9), 214–226.
Madadi, Bahman, van Nes, Rob, Snelder, Maaike, van Arem, Bart, 2020. A bi-level model to optimize road networks for a mixture of manual and automated driving: An evolutionary local search algorithm. Comput.-Aided Civ. Infrastruct. Eng. 35 (1), 80–96.
Madadi, Bahman, Van Nes, Rob, Snelder, Maaike, Van Arem, Bart, 2021. Optimizing road networks for automated vehicles with dedicated links, dedicated lanes, and mixed-traffic subnetworks. J. Adv. Transp. 2021.
Martínez-Díaz, Margarita, Al-Haddad, Christelle, Soriguera, Francesc, Antoniou, Constantinos, 2021. Platooning of connected automated vehicles on freeways: a bird's eye view. Transp. Res. Procedia 58, 479–486.
McAuliffe, Brian, Lammert, Michael, Lu, Xiao-Yun, Shladover, Steven, Surcel, Marius-Dorin, Kailas, Aravind, 2018. Influences on energy savings of heavy trucks using cooperative adaptive cruise control. SAE Technical Paper.
Metropolis, Nicholas, Rosenbluth, Arianna W., Rosenbluth, Marshall N., Teller, Augusta H., Teller, Edward, 1953. Equation of state calculations by fast computing machines. J. Chem. Phys. 21 (6), 1087–1092.
Milanés, Vicente, Shladover, Steven E., 2014. Modeling cooperative and autonomous adaptive cruise control dynamic responses using experimental data. Transp. Res. C 48, 285–300.

Molina-Masegosa, Rafael, Gozalvez, Javier, 2017. LTE-V for sidelink 5G V2X vehicular communications: A new 5G technology for short-range vehicle-to-everything communications. IEEE Veh. Technol. Mag. 12 (4), 30–39.
Mtoi, Enock T., Moses, Ren, 2014. Calibration and evaluation of link congestion functions: applying intrinsic sensitivity of link speed as a practical consideration to heterogeneous facility types within urban network. J. Transp. Technol..
Nagurney, Anna, 1998. Network Economics: A Variational Inequality Approach. vol. 10, Springer Science & Business Media.
Noruzoliaee, Mohamadhossein, Zou, Bo, Zhou, Yan Joann, 2021. Truck platooning in the US national road network: A system-level modeling approach. Transp. Res. E: Logist. Transp. Rev. 145, 102200.
Perederieieva, Olga, Ehrgott, Matthias, Raith, Andrea, Wang, Judith Y.T., 2015. A framework for and empirical study of algorithms for traffic assignment. Comput. Oper. Res. 54, 90–107.
Poorzahedy, Hossain, Abulghasemi, Farhad, 2005. Application of ant system to network design problem. Transportation 32 (3), 251–273.
Poorzahedy, Hossain, Rouhani, Omid M., 2007. Hybrid meta-heuristic algorithms for solving network design problem. European J. Oper. Res. 182 (2), 578–596.
Bureau of Public Roads, United States, 1964. Traffic Assignment Manual for Application with a Large, High Speed Computer. vol. 37, US Department of Commerce, Bureau of Public Roads, Office of Planning, Urban.
Robinson, Tom, Chan, Eric, Coelingh, Erik, 2010. Operating platoons on public motorways: An introduction to the sartre platooning programme. In: 17th World Congress on Intelligent Transport Systems. vol. 1, p. 12.
Saric, Ammar, Albinovic, Sanjin, Dzebo, Suada, Pozder, Mirza, 2019. Volume-delay functions: A review. In: Advanced Technologies, Systems, and Applications III: Proceedings of the International Symposium on Innovative and Interdisciplinary Applications of Advanced Technologies (IAT). vol. 2, Springer, pp. 3–12.
Sheffi, Yosef, 1985. Urban Transportation Networks. vol. 6, Prentice-Hall, Englewood Cliffs, NJ.
Shladover, Steven E., Nowakowski, Christopher, Lu, Xiao-Yun, Ferlis, Robert, 2015. Cooperative adaptive cruise control: Definitions and operating concepts. Transp. Res. Rec. 2489 (1), 145–152.
Shladover, Steven E., Su, Dongyan, Lu, Xiao-Yun, 2012. Impacts of cooperative adaptive cruise control on freeway traffic flow. Transp. Res. Rec. 2324 (1), 63–70.
Spiess, Heinz, 1990. Conical volume-delay functions. Transp. Sci. 24 (2), 153–158.
Spinellis, Diomidis D., Papadopoulos, Chrissoleon T., 2000. A simulated annealing approach for buffer allocation in reliable production lines. Ann. Oper. Res. 93, 373–384.
Stabler, Ben, 2018. Transportation networks for research github repository. https://github.com/bstabler/TransportationNetworks.
Tobin, Roger L., Friesz, Terry L., 1988. Sensitivity analysis for equilibrium network flow. Transp. Sci. 22 (4), 242–250.
Wadud, Zia, MacKenzie, Don, Leiby, Paul, 2016. Help or hindrance? The travel, energy and carbon impacts of highly automated vehicles. Transp. Res. A 86, 1–18.
Wang, Senlei, Correia, Gonçalo Homem de Almeida, Lin, Hai X., 2022. Assessing the potential of the strategic formation of urban platoons for shared automated vehicle fleets. J. Adv. Transp. 2022, 1–20.
Wang, Jian, Kim, Yong Hoon, He, Xiaozheng, Peeta, Srinivas, 2018. Analytical model for information flow propagation wave under an information relay control strategy in a congested vehicle-to-vehicle communication environment. Transp. Res. C 94, 1–18.
Wang, David Z.W., Liu, Haoxiang, Szeto, W.Y., 2015. A novel discrete network design problem formulation and its global optimization solution algorithm. Transp. Res. E: Logist. Transp. Rev. 79, 213–230.
Wang, Jian, Lu, Lili, Peeta, Srinivas, He, Zhengbing, 2021. Optimal toll design problems under mixed traffic flow of human-driven vehicles and connected and autonomous vehicles. Transp. Res. C 125, 102952.
Wang, Shuaian, Meng, Qiang, Yang, Hai, 2013. Global optimization methods for the discrete network design problem. Transp. Res. B 50, 42–60.
Wang, Jian, Peeta, Srinivas, He, Xiaozheng, 2019. Multiclass traffic assignment model for mixed traffic flow of human-driven vehicles and connected and autonomous vehicles. Transp. Res. B 126, 139–168.
Xiao, Lin, Wang, Meng, Schakel, Wouter, van Arem, Bart, 2018. Unravelling effects of cooperative adaptive cruise control deactivation on traffic flow characteristics at merging bottlenecks. Transp. Res. C 96, 380–397.
Yang, Hai, Huang, Hai-Jun, 2005. Mathematical and Economic Theory of Road Pricing. Elsevier.
Yao, Zhihong, Gu, Qiufan, Jiang, Yangsheng, Ran, Bin, 2022. Fundamental diagram and stability of mixed traffic flow considering platoon size and intensity of connected automated vehicles. Physica A 604, 127857.
Ye, Yipeng, Wang, Hua, 2018. Optimal design of transportation networks with automated vehicle links and congestion pricing. J. Adv. Transp. 2018.
Ye, Lanhang, Yamamoto, Toshiyuki, 2018. Modeling connected and autonomous vehicles in heterogeneous traffic flow. Physica A 490, 269–277.
Yin, Yafeng, 2000. Genetic-algorithms-based approach for bilevel programming models. J. Transp. Eng. 126 (2), 115–120.
Zeng, Tengchan, Semiari, Omid, Saad, Walid, Bennis, Mehdi, 2019. Joint communication and control for wireless autonomous vehicular platoon systems. IEEE Trans. Commun. 67 (11), 7907–7922.
Zhang, Wei, Jenelius, Erik, Ma, Xiaoliang, 2017. Freight transport platoon coordination and departure time scheduling under travel time uncertainty. Transp. Res. E: Logist. Transp. Rev. 98, 1–23.
Zhang, Xiaoning, Yang, Hai, 2004. The optimal cordon-based network congestion pricing problem. Transp. Res. B 38 (6), 517–537.
Zhao, Li, Sun, Jian, 2013. Simulation framework for vehicle platooning and car-following behaviors under connected-vehicle environment. Procedia-Social Behav. Sci. 96, 914–924.
Zhou, Jiazu, Zhu, Feng, 2021. Analytical analysis of the effect of maximum platoon size of connected and automated vehicles. Transp. Res. C 122, 102882.
Zockaie, Ali, Aashtiani, Hedayat Z., Ghamami, Mehrnaz, Nie, Yu, 2016. Solving detour-based fuel stations location problems. Comput.-Aided Civ. Infrastruct. Eng. 31 (2), 132–144.
Zockaie, Ali, Saberi, Meead, Saedi, Ramin, 2018. A resource allocation problem to estimate network fundamental diagram in heterogeneous networks: Optimal locating of fixed measurement points and sampling of probe trajectories. Transp. Res. C 86, 245–262.